JGR Oceans

RESEARCH ARTICLE
10.1029/2021JC018140

# A Potential Energy Analysis of Ocean Surface Mixed Layers

**Brandon G. Reichl[1], Alistair Adcroft[2], Stephen M. Griffies[1,2], and Robert Hallberg[1,2]**

[1]NOAA Geophysical Fluid Dynamics Laboratory, Princeton, NJ, USA, [2]Program in Atmospheric and Oceanic Sciences, Princeton University, Princeton, NJ, USA

**Key Points:**

- Diagnosing the mixed layer depth (MLD) from potential energy (PE) anomaly yields a MLD constrained by energy
- The PE-based MLD considers the integrated stratification within the mixed layer
- The PE-based MLD is strongly correlated with the active boundary layer depth

**Correspondence to:**

B. G. Reichl,
brandon.reichl@noaa.gov

**Citation:**

Reichl, B. G., Adcroft, A., Griffies, S. M., & Hallberg, R. (2022). A potential energy analysis of ocean surface mixed layers. *Journal of Geophysical Research: Oceans*, *127*, e2021JC018140. https://doi.org/10.1029/2021JC018140

Received 18 OCT 2021
Accepted 20 MAY 2022



**Abstract** Turbulent mixing in the ocean surface boundary layer leads to the presence of a surface mixed layer. This mixed layer is important for many phenomena including large-scale ocean dynamics, ocean-atmosphere coupling, and biological and biogeochemical processes. Analysis of the ocean mixed layer requires one to estimate its vertical extent, for which there are various definitions. Correspondingly, there are uncertainties on how to best identify an ocean surface mixed layer for a given application. We propose defining the mixed layer depth (MLD) from energetic principles through the potential energy (PE). The PE based MLD is based on the concept of PE anomaly, which measures the stratification of a layer of seawater by estimating its energetic distance from a well-mixed state. We apply the PE anomaly to diagnose the MLD as the depth to which a given energy could homogenize a layer of seawater. We evaluate the MLD defined by common existing methods and demonstrate that they contain a wide range of PE anomalies for the same MLD, particularly evident for deep winter mixed layers. The MLD defined from the PE anomaly ensures a more consistent MLD identified for a large range of stratifications. Furthermore, the PE method relates to the turbulent kinetic energy budget of the ocean surface boundary layer, which is fundamental to upper ocean mixing processes and parameterizations. The resulting MLD is more representative of active boundary layer turbulence, and is more robust to small anomalies in seawater properties.

**Plain Language Summary** Properties such as temperature, salinity, nutrients, and chemical and biogeochemical tracers are usually well-mixed vertically near the surface of the ocean. This layer is strongly mixed because winds, waves, and convective plumes are actively churning and stirring the near-surface fluid. Oceanographers are interested in this surface mixed layer because it plays a significant role in how the ocean works from physical, biological, and chemical perspectives. However, the boundary between the mixed layer and the interior is difficult to identify, and therefore scientists have proposed numerous methods to identify this depth. In this paper we suggest to identify the mixed layer depth (MLD) based on potential energy (PE). A well mixed column has more PE than a stratified column because it has more mass located further from the center of the Earth. The PE difference between a column and its well-mixed state is often called the PE anomaly, and the closer a column is to well-mixed the closer the PE anomaly is to zero. In this paper we show that using the PE anomaly to identify the MLD is practical and it offers conceptual benefits by directly linking to the physics of upper ocean vertical mixing.

## 1. Introduction

The near surface of the ocean is a region that is frequently subject to turbulent mixing under the action of winds, waves, and destabilizing buoyancy fluxes. This persistent and vigorous turbulent mixing is reflected in the process-oriented description of this region as the oceanic surface turbulent boundary layer. Such mixing acts to vertically homogenize scalar properties such as temperature, salinity, and other tracers. The seasonal to longer term imprints of this mixing leads to the notion of a mixed layer, which is related to but distinct from the surface turbulent boundary layer (Brainerd & Gregg, 1995; D'Asaro, 2014; Sutherland et al., 2014). The mixed layer affords an important diagnostic measure of vertical exchange and ventilation without detailed knowledge of boundary layer turbulence processes. Consequently, the mixed layer has become a central diagnostic measure of how the ocean interacts with the atmosphere and sea ice as part of the climate system.

The ocean mixed layer regulates the exchange of heat, gases, and other properties between the atmosphere and the ocean. Physical properties of this region control the magnitude of the the diurnal cycle (Price et al., 1986), provide the thermal energy available to a tropical cyclone (Ginis, 2002), and modulate the seasonal cycle (Large et al., 1994). The mixed layer transmits properties to the ocean interior through ventilation and the formation of the thermocline (Luyten et al., 1983; Williams, 1991) and through surface water-mass transformation (Groeskamp

et al., 2019). The mixed layer is also the setting of the biological pump (Franks, 2014; Gardner et al., 1995) and modulates carbon subduction to the interior (Omand et al., 2015). Descriptive and quantitative analysis of the mixed layer and mixed layer processes requires one to identify the mixed layer depth (MLD), which is the focus of this study.

### 1.1. Requirements for Defining a Mixed Layer Depth

The primary purpose of a MLD diagnostic is to identify the vertical extent where near-surface ocean properties are mixed. Mixing processes in the ocean are transient and in regular competition with restratification, such that a mixed layer is rarely perfectly homogeneous. Furthermore, observed and modeled ocean states represent either snapshots or time mean states, which are incomplete descriptions of the mixed layer and its evolution beyond a given time interval. It follows that practical mixed layer diagnostics allow for a degree of inhomogeneity, and thus the mixed layer subjectively represents a layer that recently experienced mixing or is conditioned to experience mixing in the near future.

Many scalars could be used to identify the MLD, with thermodynamic quantities such as temperature, salinity, and density commonly chosen. Identifying the MLD from density stratification physically connects the mixed layer to the turbulent boundary layer (see Section 2). These quantities are also observed and recorded globally via moorings, gliders, Argo floats, and CTD surveys, and are routinely saved as part of numerical ocean model output. While a single profile of stratification cannot indicate active mixing, it does sample the recent history of turbulent fluxes in a column via their imprint on the stratification. Therefore, defining the MLD as a region with low density stratification is a natural approach and is broadly applicable to physical, chemical, and biological mixed layer analysis.

#### 1.1.1. Threshold Based Mixed Layer Depths

The mixed layer is characterized by a well-mixed region near the surface and a transition region near the base, capping the stratification below. One method to define the MLD is to apply threshold criteria based on the vertical structure of scalar fields. The threshold method defines the MLD where the near-surface value of a chosen quantity, $\psi$, exceeds a subjectively specified threshold, $\Delta\psi$, from its surface value (de Boyer Montégut et al., 2004; Levitus, 1982):

$$\psi(z = -h_{ML}) = \psi(z = z_d) + \Delta\psi, \tag{1}$$

where $h_{ML} > 0$ is the MLD, $z_d$ is a reference geopotential position, and all functions are also dependent on time and horizontal location. A common choice for $\psi$ is potential density $\rho_\theta$, though in regions where density is dominated by temperature, such as the tropical latitudes, potential temperature $\theta$ is also used (see de Boyer Montégut et al., 2004; Holte & Talley, 2009; Thomson & Fine, 2003, for a few summaries of threshold methods).

Details of the thresholds can have sizable impacts on the diagnosed MLD and there is little physical guidance for choosing such thresholds. Many implementations of the threshold method chose a reference geopotential position of $z_d = -10$ m to reduce sensitivity to the diurnal cycle. A common threshold value is $\Delta\rho_\theta = 0.03$ kg m$^{-3}$ (de Boyer Montégut et al., 2004), empirically determined from visual inspection of ocean profiles. However, these choices can bias the method toward mid-latitude mixed layers. In particular, previous studies find that lower thresholds are needed to avoid overestimating the MLD when there is weak stratification, such as in the high-latitude winters (see Noh & Lee, 2008). Other studies find that higher thresholds are needed to avoid underestimating the MLD in shallow mixed layers, such as in the Arctic (Peralta-Ferriz & Woodgate, 2015). Hence, there is no choice that works well to identify the MLD in all regions of the ocean (see also Holte & Talley, 2009; Hosoda et al., 2010; Thomson & Fine, 2003). Despite these shortcoming, the threshold method is the standard method to estimate the MLD in the ocean component of the Coupled Model Intercomparison Project protocol (Griffies et al., 2016), which is both a result of and a perpetuation of its prevalence in the oceanographic and climate communities.

#### 1.1.2. Algorithm Based Mixed Layer Depths

There are numerous alternative methods proposed to identify the MLD in place of the threshold method. These other methods target other physical features of a water column that also characterize typical mixed layers. For example, gradient methods estimate the MLD from vertical property gradients, since stratification often

reaches a maximum value between the mixed layer and the pycnocline, thermocline, or halocline (Lukas & Lindstrom, 1991). Even considering these alternatives, no single method has been identified as a standard method to accurately estimate the MLD over the diverse combination of temperature, salinity, and density profiles found throughout the world's oceans.

Hybrid methods have emerged as a popular choice to more accurately estimate the MLD globally by combining several approaches into a single algorithmic approach. Algorithm methods analyze patterns in water column features and navigate logical decision trees to determine whether threshold, gradient, or other methods are optimal for a given regime. A popular recent algorithm approach is described in detail by Holte and Talley (2009, hereafter HT09). The HT09 algorithm approach yields a globally applicable MLD diagnostic that considers spatial and seasonal patterns of what a mixed layer usually looks like. However, the HT09 algorithm uses a multi-step decision tree that is computationally intensive to implement for evaluating many profiles, such as typically occurs with model diagnostics. Furthermore, the branches of the algorithm rely on critical thresholds like Equation 1 that are subjectively chosen. The classification scheme also creates discontinuities related to discrete boundaries between classification methods, where a continuous field is desirable.

### 1.2. Turbulent Boundary Layer Depths

The surface turbulent boundary layer depth (BLD) is the process-driven counterpart to the MLD that measures the depth that properties are actively experiencing vertical turbulent mixing. Diagnosing the BLD requires knowing turbulent quantities in the water column, such as turbulent kinetic energy (TKE), dissipation, or turbulent fluxes (see Brainerd & Gregg, 1995; Burchard, 2001; Lozovatsky et al., 2006; Sutherland et al., 2014). These turbulent properties are rarely available from field measurements or resolved by models, hence the BLD is difficult to diagnose on global scales.

Parameterizations for the BLD exist, particularly those used in numerical ocean models. These parameterizations require information such as the buoyancy and current profiles (e.g., Large et al., 1994) or the surface momentum and buoyancy fluxes (e.g., Gaspar et al., 1990; Kraus & Turner, 1967; Reichl & Hallberg, 2018) to estimate the BLD. Since ocean currents are rarely observed together with hydrographic profiles (e.g., on an Argo float, see Wong et al. (2020)), there is little opportunity for using parameterized turbulent mixing layer depths from observations globally. Observational analysis of the boundary layer is therefore limited to specific stations/times when sufficient measurements are taken.

Even if we had information needed to diagnose the BLD, would the BLD be preferable to the MLD, where the MLD measures the depth over which active turbulent mixing is imprinted on scalar properties? If interested in direct effects of turbulent mixing, knowing the BLD is important. However, for large-scale questions over seasonal to climate time scales, we propose that the MLD is a more relevant measure of ocean mixing and its associated ventilation. The difference is whether we are interested in the turbulent processes themselves or with their effects on the evolution of ocean properties, such as ocean interior heat and carbon concentrations.

### 1.3. An Improved, Energy Based Method to Define the Mixed Layer

The reason that existing methods contain arbitrary, subjective thresholds to define the MLD is that they are not directly related to the physical principles that underpin ocean boundary layer mixing. In this paper, we incorporate a basic understanding of turbulent mixing energetics as part of a proposed new MLD diagnostic. We demonstrate that the potential energy (PE) of the ocean column is a suitable basis to diagnose the MLD and offers significant physical and conceptual benefits compared to previous methods. The resulting energetically based MLD directly aligns with the physics of boundary layer turbulence while remaining a practical diagnostic for observations and numerical models. The proposed MLD is physically interpreted as the depth to which a given energy could homogenize a column of seawater. The threshold energy value in the PE based MLD is connected to mixing energetics and thus offers a physical basis for its choice.

We report details of the new method in this manuscript. First, in Section 2 we review the energetics of the turbulent ocean surface boundary layer to introduce the concept of PE anomaly. In Section 3 we use the PE anomaly to examine the stratification in the mixed layer identified by common existing MLD methods. This analysis motivates us to propose a new MLD method that directly considers the PE anomaly of the mixed layer. Finally,

**Table 1**
*Table of Variables and Their Definitions as Used in This Paper*

| Variable | Definition | MKS units |
|---|---|---|
| $\epsilon$ | TKE dissipation rate | $m^2\ s^{-3}$ |
| $\eta$ | sea surface elevation above geoid | m |
| $\varphi$ | potential energy anomaly | $J\ m^{-2}$ |
| $\rho$ | in situ density | $kg\ m^{-3}$ |
| $\rho_0$ | constant reference density | $kg\ m^{-3}$ |
| $\rho_\theta$ | potential density | $kg\ m^{-3}$ |
| $\Theta$ | Conservative Temperature | °C |
| $b$ | buoyancy $(-g(\rho/\rho_0 - 1))$ | $m\ s^{-2}$ |
| $g$ | gravitational acceleration | $m\ s^{-2}$ |
| $h$ | depth $(h = -z)$ | m |
| $h_{ML}$ | mixed layer depth (MLD) | m |
| $k$ | turbulent kinetic energy (TKE) (per unit mass) | $m^2\ s^{-2}$ |
| $K_H$ | turbulent diffusivity | $m^2\ s^{-1}$ |
| $K_M$ | turbulent viscosity | $m^2\ s^{-1}$ |
| $N^2$ | Brunt-Väisälä frequency | $s^{-2}$ |
| $P_g$ | gravitational potential energy | $J\ m^{-2}$ |
| $S$ | Absolute Salinity | $g\ kg^{-1}$ |
| $u_i$ | components of 3d velocity vector | $m\ s^{-1}$ |
| $w = u_3$ | vertical velocity component | $m\ s^{-1}$ |
| $x_i$ | components of 3d position vector | m |
| $z = x_3$ | vertical position (positive up) | m |
| $z_c$ | column center of mass (positive up) | m |
| $z_d$ | threshold vertical position (positive up) | m |
| $z_r$ | reference vertical position (positive up) | m |

we investigate various implementation choices for this method (Section 4) and offer recommendations for its general use. Appendix A provides some comments on the Boussinesq approximation, and Appendix B offers guidance for understanding the values for the energies considered in the MLD diagnostic.

## 2. Energy in Mixed Layers and Turbulent Boundary Layers

In this section we discuss how the PE can be used to describe the stratification of a seawater column. We begin by reviewing the energetics of the formation and maintenance of an ocean mixed layer. The connection between the budgets for PE and TKE highlights the physical basis behind the PE method later proposed to define mixed layer depths.

### 2.1. The Turbulent Buoyancy Flux Converts Between TKE and PE in a Water Column

The one-dimensional TKE budget for the surface boundary layer describes the production, dissipation, and vertical transport of energy (see Rodi, 1987), while neglecting horizontal processes. The vertically integrated TKE budget from an arbitrary vertical position, $z = -h$, to the ocean surface, $z = \eta$, is given here in a form that neglects temporal changes in $\eta$ and $h$ and neglects TKE fluxes across the integration bounds:

$$\frac{\mathrm{d}}{\mathrm{d}t}\left(\int_{-h}^{\eta} \overline{k}\,\mathrm{d}z\right) = \int_{-h}^{\eta}\left(-\overline{w'u_i'}\partial_z\overline{u}_i + \overline{w'b'} - \epsilon\right)\mathrm{d}z, \tag{2}$$

where

$$\overline{k} = \overline{u_i'u_i'}/2 \tag{3}$$

is the TKE per unit mass (see Table 1 for a list of symbols used in this paper), and the Einstein summation convention is assumed when indices are repeated. Summations are taken over three index dimensions in Equation 3, but since the boundary layer approximation is already taken in Equation 2 only the two horizontal indices are summed. The mean fields are determined by an averaging filter denoted by an overbar $(\overline{\psi})$, which formally represents the mean over an ensemble of realizations (see chapter 13 of Kundu and Cohen (2007) or Tennekes and Lumley (1972) for a thorough introduction). Turbulent fields $(\psi')$ are then defined as the difference between the full field and the mean $(\psi' = \psi - \overline{\psi})$. The TKE budget Equation 2 includes three terms on the RHS that may increase or decrease turbulence (TKE) in a seawater layer. Additional TKE sources and sinks are not precluded from this discussion and could be introduced through boundary conditions or additional physical processes such as Stokes production (e.g., Reichl & Li, 2019).

The first term on the RHS in Equation 2 is the integrated shear-production $-\overline{w'u_i'}\partial_z\overline{u}_i$, which is a TKE source. The downgradient form of shear-production is introduced by defining a variable eddy-viscosity, $K_M$:

$$-\overline{w'u_i'}\partial_z\overline{u}_i = K_M\left[\left(\partial_z\overline{u}_1\right)^2 + \left(\partial_z\overline{u}_2\right)^2\right] = K_M\,S^2, \tag{4}$$

where

$$S^2 = \left(\partial_z\overline{u}_1\right)^2 + \left(\partial_z\overline{u}_2\right)^2 \tag{5}$$

is the squared mean shear frequency. This term is sign definite for positive values of $K_M$, hence the shear production is usually taken to be a TKE source. The final term in Equation 2 is the dissipation, $\epsilon > 0$, which represents a loss of TKE to viscous dissipation.

The second term in Equation 2 is the buoyancy flux, $\overline{w'b'}$, which can also be described by a downgradient form for conceptual purposes with variable eddy-diffusivity, $K_H$:

$$\overline{w'b'} = -K_H\, \partial_z \overline{b} = -K_H\, N^2, \tag{6}$$

where

$$N^2 = \partial_z \overline{b} = -(g/\rho_0)\, \partial_z \overline{\rho} \tag{7}$$

is the squared buoyancy frequency of the mean state. The buoyancy flux is not sign-definite even when assumed downgradient, for example, it can be a source of TKE when $N^2 < 0$ (unstable stratification) and a sink of TKE when $N^2 > 0$ (stable stratification). The downgradient assumption yields conceptual benefits, and while it may be unphysical during convection the general relationships between the sign of the buoyancy flux and the TKE budget hold. The TKE loss in stable stratification is usually a much smaller sink than dissipation, often more than an order of magnitude smaller, where $\overline{w'b'}/\epsilon \leq 0.2$ in stably stratified turbulence (e.g., Osborn, 1980). However, the buoyancy flux is central to our purposes since it connects the TKE budget to the gravitational PE of a water column.

The gravitational PE per horizontal area, $P_g$, of a fluid column is determined by its mass (per unit area) and the position of its center of mass along the axis of gravity. This can be summarized in integral form from the in situ density profile as:

$$P_g = \int_{-h}^{\eta} \rho\, g\, (z - z_r)\, \mathrm{d}z, \tag{8}$$

where $\eta$ and $h$ are the same integration bounds as in Equation 2 and the remaining variables are defined in Table 1. While the PE budget contains numerous terms, the contribution of vertical mixing is realized as:

$$\frac{\mathrm{d}P_g}{\mathrm{d}t} = \ldots\ - \rho_0 \int_{-h}^{\eta} \overline{w'b'}\, \mathrm{d}z. \tag{9}$$

We here see that the buoyancy flux contributes oppositely to the mean PE in Equation 9 relative to the TKE in Equation 2. Hence, the turbulent buoyancy flux converts between kinetic energy in turbulence and mean PE (see Burchard, 2002, for a detailed discussion of the upper ocean energy budget).

### 2.2. The PE Anomaly Measures the Integrated Effects of Stratification

The particularly simple form of the PE budget in the previous subsection (Equation 9) motivates us to use the PE to measure vertical stratification in the water column. We achieve this aim by computing the PE difference between a given state and its corresponding fully mixed state, thus connecting the stratification to the energetics of turbulence in Equation 2.

The tendency of $P_g$ can be found directly by taking the time derivative of Equation 8:

$$\frac{\mathrm{d}P_g}{\mathrm{d}t} = \frac{\mathrm{d}}{\mathrm{d}t}\left[\int_{-h}^{\eta} \rho\, g\, (z - z_r)\, \mathrm{d}z\right]. \tag{10}$$

Estimating this time tendency from repeated density profiles would yield information about turbulent mixing directly from only the density. However, subsequent profiles of density are not always readily available, for example, an Argo float only makes one measurement per 10 days. Even if subsequent profiles are available, the impacts of boundary fluxes and lateral processes in observations can be difficult to untangle from the mixing, and thus we prefer a simpler approach. Therefore we evaluate the time integral of Equation 10 from the current time, $t = t_i$, to a specific, hypothetical future time, $t = t_m$. In the absence of forcing, the maximum achievable value of this time integral for a stable future state is the difference in the PE per unit area of the mixed state relative to the current state:

$$\Delta P_g = \overbrace{\int_{-h}^{\eta_m} g\,\rho_m\,(z - z_r)\,\mathrm{d}z}^{\text{PE at Mixed State } t_m} - \overbrace{\int_{-h}^{\eta_i} g\,\rho_i\,(z - z_r)\,\mathrm{d}z}^{\text{Current State } t_i}. \tag{11}$$

The maximum PE state that a column of seawater can evolve to without a mean external forcing is one where all scalar properties (notably Conservative Temperature, $\Theta$, and Absolute Salinity, $S$) are well-mixed from $-h$ to $\eta$. $\rho_m$ is thus the in situ density profile corresponding to the well-mixed state of the column, where $\rho_m$ is not generally uniform vertically since pressure is a function of depth in the column. Furthermore, $\eta_m$ accounts for changes in the volume of the water column as a result of changing its in situ density due to the non-linear equation of state. This relationship is valid for non-Boussinesq fluids only (see Appendix A), so that implementation of this diagnostic for Boussinesq models must account for the volume expansion.

The reference level, $z_r$, in Equation 11 is arbitrary and drops out from the $\Delta P_g$ calculation due to mass conservation between the initial and mixed state. The cancellation is trivial to show when written in (hydrostatic) pressure coordinates (with $\mathrm{d}p = -g\,\rho\,\mathrm{d}z$), where the pressure integration bounds are stationary in time with respect to mixing within the column:

$$\Delta P_g = -\left( \overbrace{\int_{p_b}^{p_t} (z_m - z_r)\,\mathrm{d}p}^{\text{PE at Mixed State } t_m} - \overbrace{\int_{p_b}^{p_t} (z_i - z_r)\,\mathrm{d}p}^{\text{Current State } t_i} \right) = -\int_{p_b}^{p_t} (z_m - z_i)\,\mathrm{d}p. \tag{12}$$

In this equation, $z$ is the vertical position as a function of pressure (for the initial, $z_i$, and final, $z_m$, state), whereas $p_t$ and $p_b$ are the top and bottom hydrostatic pressures. An equivalent form of Equation 12 using the specific volume, $\alpha = 1/\rho$, is particularly useful for accurately and efficiently calculating PE changes due to mixing in numerical models:

$$\Delta P_g = -\int_{p_b}^{p_t} (\alpha_m - \alpha_i)\,\frac{p}{g}\,\mathrm{d}p, \tag{13}$$

where this equality holds when assuming a vanishing surface pressure (this form of the PE change underpins the energetically constrained surface mixing parameterization described by Reichl and Hallberg (2018)). Equations 11–13 formally yield the mechanical energy required to mix the water column from its current stratified state to its maximum PE homogeneous state, giving the work associated with raising the center of mass.

For this discussion we have assumed that the initial state for the column is statically stable, and thus that the homogeneous layer would have more PE than the initial state. In convectively unstable situations (e.g., high-latitude winter or night time) the initial state can have more PE than the mixed state. This situation indicates that the column has energy available to convert to turbulence.

### 2.3. The Simplified Potential Energy Anomaly, $\phi$

Using the PE budget to characterize a mixed layer is similar to studies that define a PE anomaly, $\phi$, to assess stratification in a water column (e.g., Burchard & Hofmeister, 2008; Simpson, 1981). However, Equation 11 is not identical to this usual PE anomaly. The two can only be treated equivalently after making certain assumptions about the fluid and its equation of state.

The traditional definition of $\phi$ comes from assuming the homogenized state is defined by directly averaging the potential density

$$\phi = \int_{-h}^{\eta} \left(\rho_\theta^m - \rho_\theta^i\right)\,g\,z\,\mathrm{d}z, \tag{14}$$

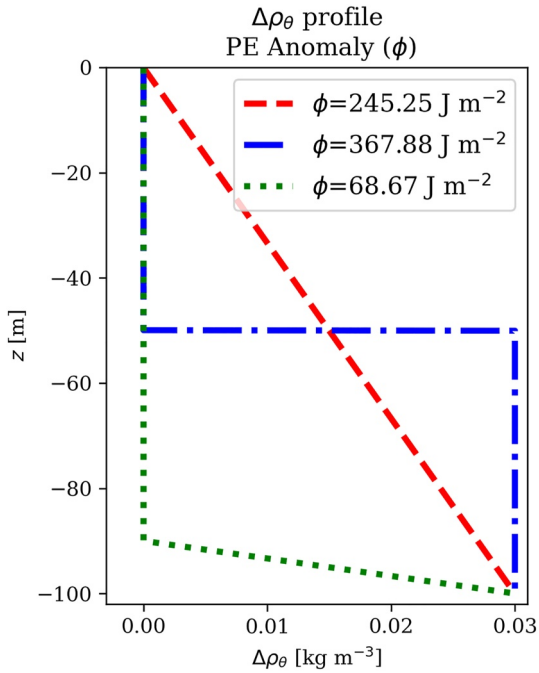


**Figure 1.** Profiles for linear (red-dashed), 2-layer (blue dash-dotted) with the layers of equal size, and fully mixed for 90% of the mixed layer with linear stratification below (green dotted). The legend gives the potential energy anomaly, $\phi$, which is determined by the difference between the given profile and its counterpart that is perfectly homogenized in potential density. For computing the threshold mixed layer depth we set reference $z_d = 0$ for simplicity. The two-layer (blue/dash-dot) curve is constructed so that the lower layer is below the threshold density by a small value until exactly 100 m depth. The linear red/dash curve reaches a potential density at 100 m that is 0.03 kg m$^{-2}$ greater than the surface. The partially mixed (green/dot) curve is similar to the linear except that the linear portion is only applied to the bottom 10% of the column and the column is homogeneous in potential density for depths shallower than 90 m.

where the reference state $z_r$ does not appear because the $z$-integral of $\rho_\theta^i$ and $\rho_\theta^m$ are identical by definition

$$\rho_\theta^m \equiv \frac{1}{\eta + h} \int_{-h}^{\eta} \rho_\theta^i \, dz. \tag{15}$$

Both the PE anomaly, $\phi$, and $\Delta P_g$ have dimensions of energy per area, which are either directly or approximately related to the energy required to mix the fluid. For the case of $\Delta P_g$, it is exactly the energy requirement to homogenize the column between $z = -h$ and $z = \eta$. In contrast, $\phi$ makes several approximations by assuming potential density is directly homogenized in the fully mixed state. With a nonlinear seawater equation of state, this approach can vary in accuracy when compared to averaging the seawater constituents within a particular water column. These approximations are accounted for in the dynamic $\phi$ equation of Burchard and Hofmeister (2008) by their term "G" in their Equation 15. Because $\phi$ is computed by volume averaging $\rho_\theta$ directly, rather than from the $\rho_\theta$ resulting from the directly averaged constituents (which are not generally the same), $\phi$ bypasses concerns between Boussinesq and non-Boussinesq models (see Appendix A), though it is inconsistent with the model energy budget except when simplified forms of the equation of state are assumed. Despite these assumptions, we later show that results derived using $\phi$ are usually consistent with those from $\Delta P_g$ for applications related to typical surface mixed layers observed in the ocean.

## 3. The Mixed Layer Potential Energy Anomaly

The concept of PE anomaly and $\Delta P_g$ metrics that describe ocean stratification have now been introduced along with their connection to boundary layer turbulence. In this section we apply PE based diagnostics to first characterize and then to define the ocean surface mixed layer.

### 3.1. Characterizing a Mixed Layer From PE Anomaly

Yamaguchi et al. (2019) recently applied the budget equation for $\phi$ to analyze the seasonal evolution of North Pacific stratification. For their approach, $h$ in Equation 14 is estimated using the threshold method MLD (with 0.03 kg m$^{-3}$ density criteria). Here we use a similar strategy to demonstrate the sensitivity of $\phi$ to various stratification configurations that yield the same threshold method MLD. Although in this exercise we only investigate sensitivity of $\phi$, we later demonstrate that $\phi$ is usually consistent with the in situ density based $\Delta P_g$. Hence, the limitations in the threshold method MLD found here with $\phi$ extend to the general case.

#### 3.1.1. Density Threshold Method Can Yield Same MLD for Distinct Stratifications

In Figure 1, we consider three physically plausible potential density profiles that yield the same MLD, $h_{ML} = 100$ m, using the threshold method with a potential density difference of 0.03 kg m$^{-3}$. The corresponding values of the PE anomalies, $\phi$, range between 70 J m$^{-2}$ and 370 J m$^{-2}$. For a reference, approximately 100 J m$^{-2}$ of kinetic energy is converted to PE when a 12 m/s wind blows over a section of ocean for about 1 day (see Appendix B for more context of these energy values). We thus see that the threshold method yields different PE anomalies, and thus different levels of stratification within equivalent mixed layers. We conclude that the threshold method for diagnosing the mixed layer is unable to distinguish between fundamentally distinct vertical stratifications.

Note that the MLD for the two-layer (blue/dash-dot) curve in Figure 1 would be better measured by reducing the threshold value from 0.03 kg m$^{-3}$ to capture the apparent MLD value of 50 m. Even so, a similar exercise could be taken where the lower layer potential density is similarly reduced, meaning that this modified threshold is not general. A more refined algorithm approach, such as HT09, could find the apparent MLD of 50 m by choosing the location of maximum density gradient in the two-layer case.

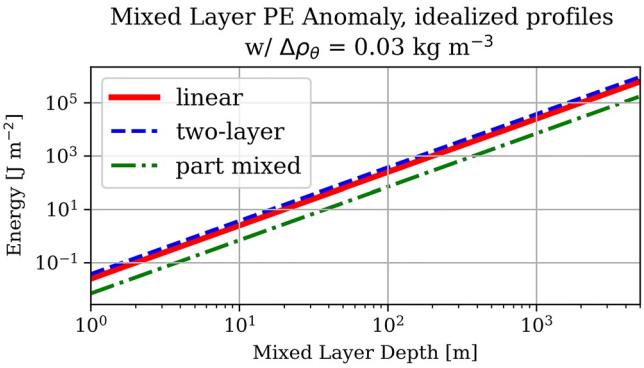


**Figure 2.** Energetic requirement to perfectly homogenize a weakly-stratified mixed layer as a function of layer thickness for potential density profiles corresponding to the colors in Figure 1. Note the log scales on both axes.

#### 3.1.2. Energetic Requirements to Homogenize to a Specified $h_{ML}$

We now consider how the PE anomaly would change in the profiles shown in Figure 1 if the $h_{ML}$ used for the threshold method is varied from 1 to 4,000 m. In each case, the profiles remain consistent as pictured in Figure 1, except they are stretched in the vertical to satisfy the range of mixed layer depths. As seen in Figure 2, we find an offset in $\phi$ for a given $h_{ML}$ (along the $y$-axis) depending on specifics of the profile (as described by Figure 1). However, there is a huge variation in $\phi$ with changing $h_{ML}$ (along the $x$-axis) for each of the three profiles. We see that for deeper mixed layer depths the energy requirement to homogenize what was identified as the "mixed" layer can become increasingly large, with the threshold criteria exceeding $10^5$ J m$^{-2}$ for all profiles down to a depth of 4,000 m. Finding a MLD of 4,000 m from the 0.03 kg m$^{-3}$ potential density threshold method is rare in nature, but it is a plausible MLD during intense deep water formation events in the high latitudes (such as a polyna).

As revealed in the first example of Figure 1, the MLD evaluated using the threshold criteria generally contains significant stratification from the perspective of the PE anomaly. The fundamental problem with the threshold based MLD is that it does not account for the PE implications of interchanging fluid elements of different density over distances along the vertical axis against gravity. The threshold method thus misses a key energetic constraint, whereby the resistance to mixing depends not only on the density difference but also on the physical distance.

We also draw attention to the shallower MLDs (between 1 and 10 m) defined from the threshold method 0.03 kg m$^{-3}$ criteria that require less than 10 J m$^{-2}$ of energy to homogenize. In many implementations of the threshold method, the reference position is taken as $z_d = -10$ m, thus these shallow MLDs are not even achievable. However, some regions of the world (e.g., the Arctic) regularly have MLDs shallower than 10 m, and accurately characterizing these MLDs is important for understanding mixed layer processes. This exercise therefore also demonstrates that the threshold method may incorrectly estimate the MLD in shallow mixing regions by identifying mixed layer depths that are very sensitive to the threshold value and reference level, with highly variable energetic implications.

#### 3.1.3. Realistic Profiles for the World Ocean

To provide global context on the PE analysis of threshold MLDs, we use a gridded Argo-based monthly temperature/salinity product (see Roemmich and Gilson (2009), obtained from https://sio-argo.ucsd.edu/RG_Climatology.html) to estimate potential density profiles globally on a 1° × 1° grid. This Argo product gives a reasonable estimate of $\Theta$, $S$ profiles, though the spatial and temporal interpolation between measurements occasionally produces stratification artifacts above the pycnocline. The gridded product is interpreted as a monthly average of density profiles, and therefore is expected to be more diffuse than individual profiles. In other words, the monthly mean MLD should be defined when possible as the monthly mean of the MLD and not the MLD of the monthly mean profile. However, the complete and gridded nature of this data set make it a qualitatively useful tool for the present demonstration. We use this product to estimate the threshold method MLD (diagnosed with the $\Delta\rho_\theta = 0.03$ kg m$^{-3}$), the HT09 MLD, and the associated value of $\phi$ for each computed MLD at each grid point for all months from 2004 to 2020.

In Figure 3 we show the 10th percentile of the time series of threshold method MLDs and corresponding values of $\phi$, which approximately represents Summer conditions. For these shallow MLDs we find small variation in $\phi$, or the amount of energy needed to mix through the stratification within the diagnosed mixed layer. However, for the 90th percentile values (which approximately represent Winter conditions, Figure 4), we see the energy needed to mix to the threshold MLD exceeds 1,500 J m$^{-2}$. In both cases we see that the HT09 algorithm MLD yields smaller values of $\phi$ than the threshold method for the deep MLDs (Figures 3 and 4, lower panels). Yet, the HT09 algorithm MLD still yields significant variations in latitude for the energy needed to mix through the stratification in the diagnosed mixed layer. Further, there are wide-swaths of the lower-latitude oceans where the HT09 algorithm predicts a MLD with greater PE anomaly than the threshold method.

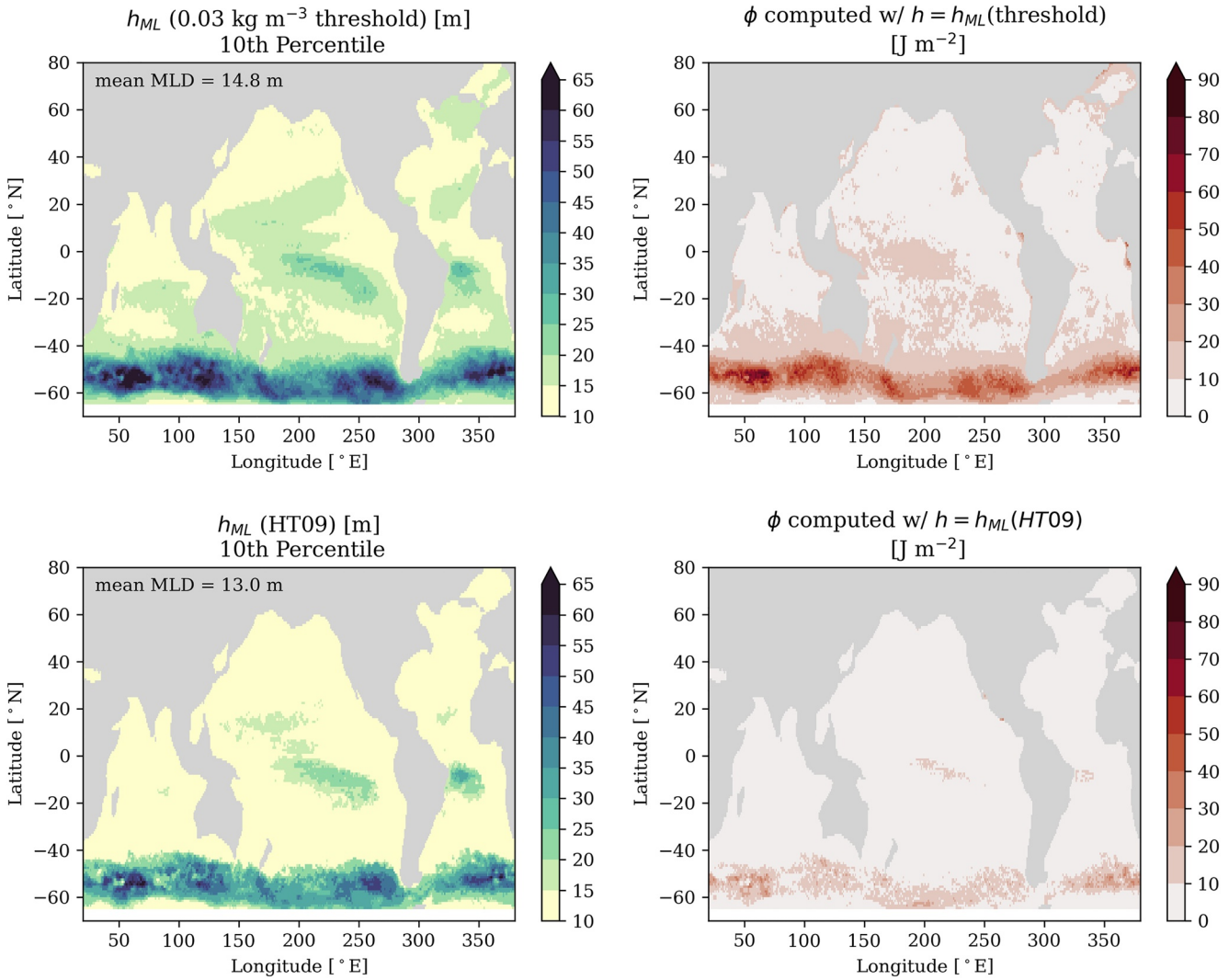


**Figure 3.** Left column: The 10th percentile (Summer) mixed layer depth (MLD) $h_{ML}$ defined using the 0.03 kg m$^{-3}$ density difference criteria (top) and the HT09 algorithm method (bottom). Right column: The 10th percentile (Summer) potential energy (PE) anomaly of the mixed layer defined using the method in the left column. MLD and PE anomalies are computed from the Argo gridded data product of Roemmich and Gilson (2009), obtained from https://sio-argo.ucsd.edu/RG_Climatology.html.

### 3.2. Defining the MLD From Potential Energy Anomaly

The threshold method for defining the MLD, $h_{ML}$, is convenient for its simplicity, but we have now demonstrated a weakness that it only considers the discrete density difference as a proxy for stratification and does not consider the integrated depth distribution of density. The HT09 algorithm identifies MLDs with smaller $\phi$ than the threshold method in deep MLD scenarios, but still these MLDs have significant variation in $\phi$.

To better consider variability in stratification within the mixed layer, we propose to instead define $h_{ML}$ to satisfy a prescribed value for the PE anomaly. That is, we modify Equation 11 by replacing the lower integral bound with the MLD:

$$\Delta P_g = \int_{-h_{ML}}^{\eta_m} \rho_m \, (z - z_r) \, g \, \mathrm{d}z - \int_{-h_{ML}}^{\eta_i} \rho_i \, g \, (z - z_r) \, \mathrm{d}z, \tag{16}$$

and the same to Equation 14:

$$\phi = \int_{-h_{ML}}^{\eta} \left(\rho_\theta^m - \rho_\theta^i\right) \, g \, z \, \mathrm{d}z. \tag{17}$$

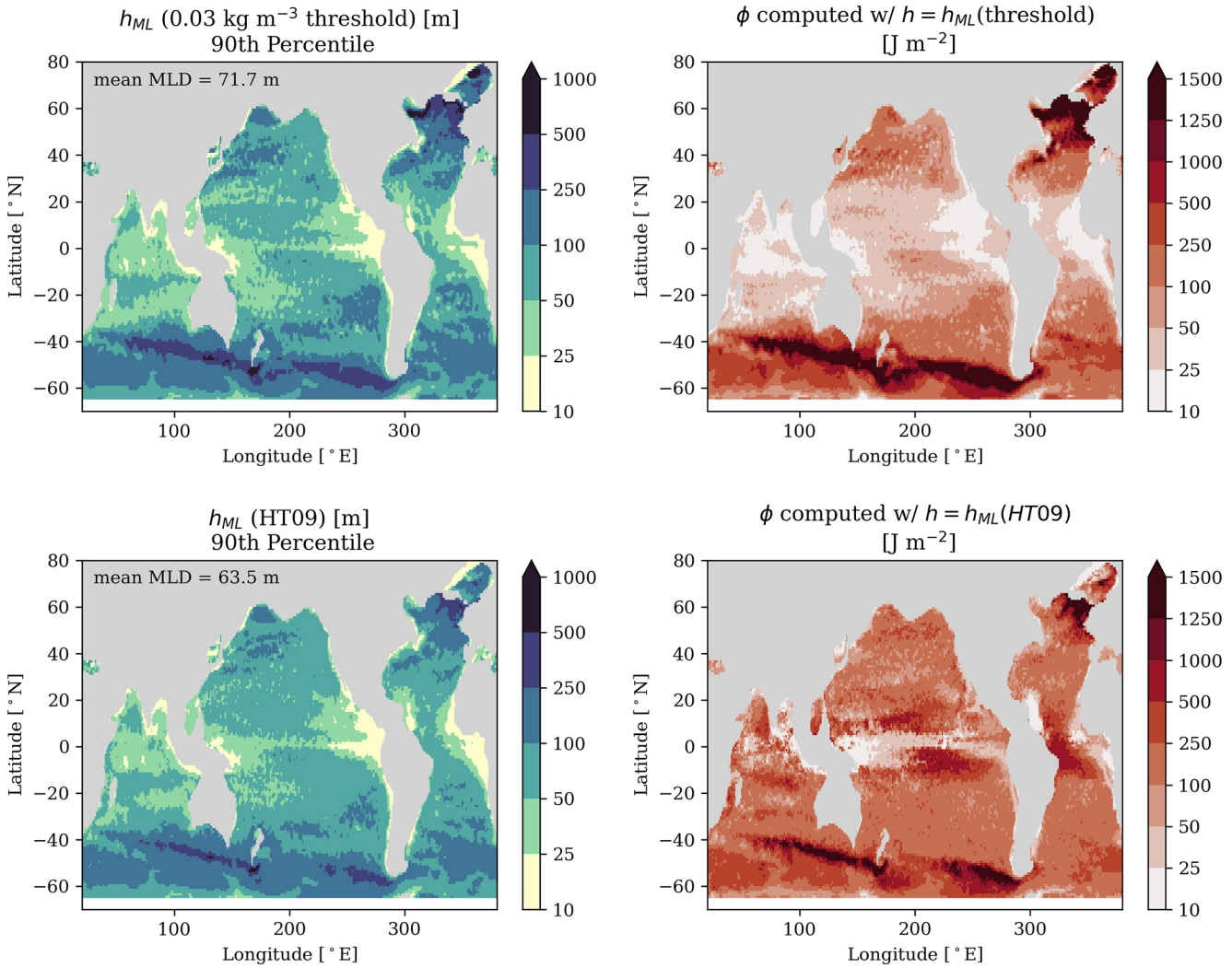


**Figure 4.** Left column: The 90th percentile (Winter) mixed layer depth (MLD), $h_{ML}$, defined using the 0.03 kg m$^{-3}$ density difference criteria (top) and the HT09 algorithm method (bottom). Right column: The 90th percentile (Winter) potential energy (PE) anomaly of the mixed layer defined using the method in the left column. MLD and PE anomalies are computed from the Argo gridded data product of Roemmich and Gilson (2009), obtained from https://sio-argo.ucsd.edu/RG_Climatology.html.

The traditional $\phi$ calculation computes $\rho_\theta^m$ and $\phi$ from a given value of $h_{ML}$ (or $\Theta_m$, $S_m$, and $\Delta P_g$), since these quantities are interrelated (e.g., as in the previous section). We propose that instead of providing the value $h_{ML}$, we can provide the value of $\phi$ (or $\Delta P_g$) and solve for a value $h_{ML}$ corresponding to the prescribed energy. Through this PE-based approach, the MLD calculation is improved to consider an integrated depth distribution of the density. These equations are usually applied to discrete measurements and not integrable functional forms, complicating solving for $h_{ML}$ directly. However, iterative techniques can be applied to a high degree of accuracy to solve for $h_{ML}$ with a given value of $\Delta P_g$ or $\phi$.

Using $\phi$ or $\Delta P_g$ to define the MLD is physically grounded from energetic constraints. However, this approach still requires choosing a dimensional criteria. This $\phi$ or $\Delta P_g$ criteria has a clear physical meaning from a boundary layer turbulence perspective; that is, it tells how deep a given amount of energy can homogenize a water column. The precise energy value could be chosen from theoretical or climatological arguments. For example, in a TKE-based surface boundary layer parameterization, the evolution of TKE and PE is predicted following equations similar to Equation 2. In convectively unstable situations, mixing can release TKE that can be available to increase PE further down in the water column (penetrative convection). We do not apply special treatment to

the convectively unstable columns in our method, such that the presence of unstable water near the surface will lead to a deeper MLD.

One solution to justify the choice for $\phi$ and $\Delta P_g$ is to relate the energy value to the local wind, wave, or surface buoyancy flux conditions. This approach relates mixing to non-dimensional threshold values based on physics, such as the $m_*$ and $n_*$ parameters in bulk mixed layer parameterizations (Kraus & Turner, 1967; Reichl & Hallberg, 2018). These parameterizations estimate when there is more (less) energy to produce a deeper (shallower) turbulent boundary layer. However, we prefer a method to estimate MLDs from observed temperature and salinity profiles from Argo profiles without requiring additional data. Therefore, we choose to have the only independent variables in our approach be the temperature and salinity profiles. While we explore recommended ranges of energy $\Delta P_g$ or $\phi$ in this study, we emphasize that the degree of inhomogeneity allowed in a mixed layer (and hence the precise energy value) may differ for different applications. Sensitivity to choices for $\Delta P_g$ and $\phi$ is given in Section 4.3. For demonstration, we use a value of 10 J m$^{-2}$ unless otherwise specified in the next several sections (see Appendix B for context of the energy values).

## 4. Analysis of the PE Based Surface Mixed Layer Depth

In the previous sections we have introduced how the PE anomaly can be used to measure the stratification of a seawater column. We then demonstrated how the PE anomaly can be used to define the MLD. In this section we analyze the sensitivity of this method to specific choices, including when $\phi$ is an approximation for $\Delta P_g$ and a brief analysis of the sensitivity of the PE based MLD to the chosen energy value.

### 4.1. Comparing PE Anomaly $\phi$ With Full Calculation $\Delta P_g$

In this section we explore the differences between using $\Delta P_g$ (Equation 16) and $\phi$ (Equation 17) to solve for $h_{ML}$. To briefly recap the differences, $\phi$ computes the PE anomaly assuming the potential density is directly homogenized whereas $\Delta P_g$ computes the PE change after homogenizing $\Theta$ and $S$ separately. Since the equation of state is a nonlinear function of $(\Theta, S, p)$, $\phi$ is not equivalent to $\Delta P_g$. However, since only one quantity is homogenized in the calculation to solve for $h_{ML}$ using $\phi$, the method is simpler to implement. Using $\phi$ is therefore the preferred method when it yields a similar result to $\Delta P_g$. We show that for most practical applications, using $\phi$ gives a similar result to using $\Delta P_g$.

We now compare the value of $h_{ML}$ predicted using the $\phi$ and $\Delta P_g$ methods utilizing a selection of idealized profiles. In Section 3.1 we specified profiles of $\rho_\theta$ directly, but here we specify profiles of Conservative Temperature $\Theta$ and Absolute Salinity $S$ to compute $\rho$ from a realistic equation of state (see Feistel (2008) and https://teos-10.github.io/GSW-Python/intro.html). We construct three profiles, which include (see Figure 5) a constant $\Theta$ gradient (red dashed), a two-layer $\Theta$ profile (blue dot-dashed), and a profile that is well-mixed near the surface with a constant $\Theta$ gradient below (green dotted). In each case Absolute Salinity $S$ is held constant at 35 g kg$^{-1}$. The structure of each $\Theta$ profile was selected so it satisfies a threshold method $h_{ML}$ of 100 m.

In the previous application (Figure 1) we computed $\phi$ due to mixing the column to 100 m, but here we compute $h_{ML}$ from each profile using both the $\Delta P_g$ approach (upper left panel, Equation 16) and the $\phi$ approach (upper right panel, Equation 17). In both cases we specify an energy value of 10 J m$^{-2}$ to solve for $h_{ML}$, which (as demonstrated later) is roughly consistent with $h_{ML}$ computed from the 0.03 kg m$^{-3}$ potential density threshold method. Both the $\phi$ and $\Delta P_g$ methods yield similar MLDs for all three profiles, notably 34.70–34.72 m for the linear profile, 51.39–51.40 m for the two-layer profile, and 93.90–93.91 m for the partially mixed profile. The similarity supports the notion that the approximation to use $\phi$ instead of $\Delta P_g$ is accurate to compute the MLD from these three profiles. We also note that both energy methods estimate MLDs closer to those that would be visually chosen for these profiles (e.g., about 50 m for the two-layer profile). These MLDs are always less than 100 m, which is the MLD in all cases using the threshold method.

The above exercise demonstrates cases where $\phi$ and $\Delta P_g$ yield similar results. We now demonstrate idealized cases where $\phi$ and $\Delta P_g$ yield different results. For this demonstration we specify two additional idealized profiles. First, we mimic a high-latitude winter density profile by specifying a profile with $\Theta = 4$°C above 500 m and $\Theta = 2$°C below 500 m (blue dotted curves, Figure 5, lower panels). Second, we mimic a low-latitude density profile with a constant $d\Theta/dz$ from $\Theta = 25$°C at the surface to $\Theta = 2$°C below 500 m (red dashed curves, Figure 5,

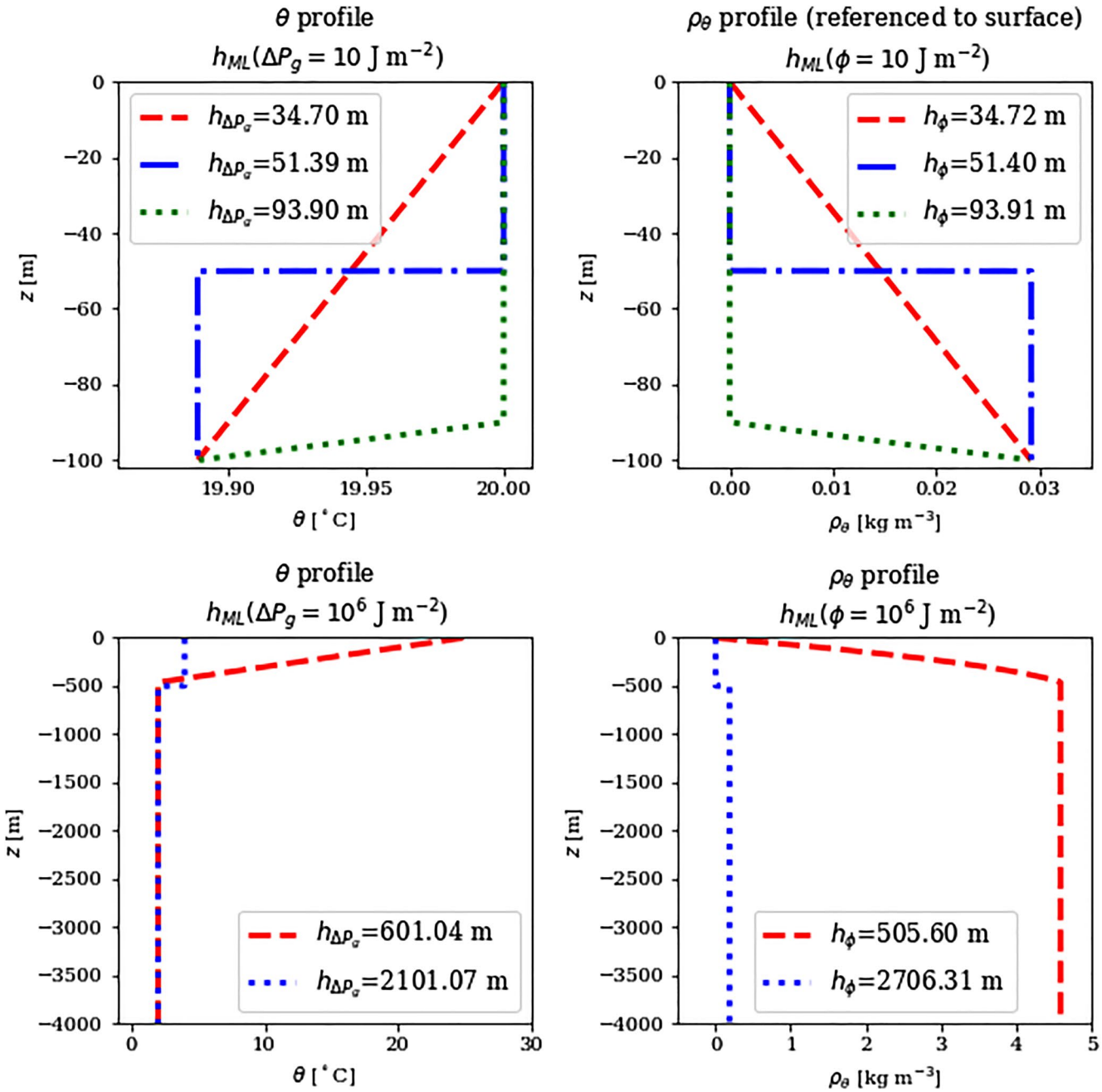


**Figure 5.** Comparing the calculation of $h_{ML}$ from the potential energy metrics of $\Delta P_g$ (Left column) and $\phi$ (Right column). Top panels: Three relatively shallow profiles that yield $h_{ML}$ = 100 m with the threshold method and the corresponding $\Theta$ (left) and potential density profiles referenced to the surface (right). The legend gives the computed $h_{ML}$ from the $\Delta P_g$ (left) and $\phi$ (right) methods, respectively. Bottom panels: Two deep profiles that yield significantly different values of $h_{ML}$ when computed from $\Delta P_g$ (left) and $\phi$ (right).

lower panels). The value $h_{ML}$ using $\phi$ and $\Delta P_g$ is similar for both profiles for energies from $1-10^4$ J m$^{-2}$ (see Figure 6). However, providing $>10^5$ J m$^{-2}$ of energy exposes cases where $\phi$ and $\Delta P_g$ yield different results (emphasized by providing the values directly for $10^6$ J m$^{-2}$ in the lower panels of Figure 5).

The error from using $\phi$ in place of $\Delta P_g$ therefore increases as the energy is increased. The error becomes greater than a few percent in these profiles when the energy exceeds $10^5$ J m$^{-2}$. For energies less than $10^4$ J m$^{-2}$ the error is less than one percent in both cases, suggesting that the approximation of using $\phi$ can be taken to be a very good one with energies less than 100 J m$^{-2}$. However, if using large energy values that penetrate to large pressures, the

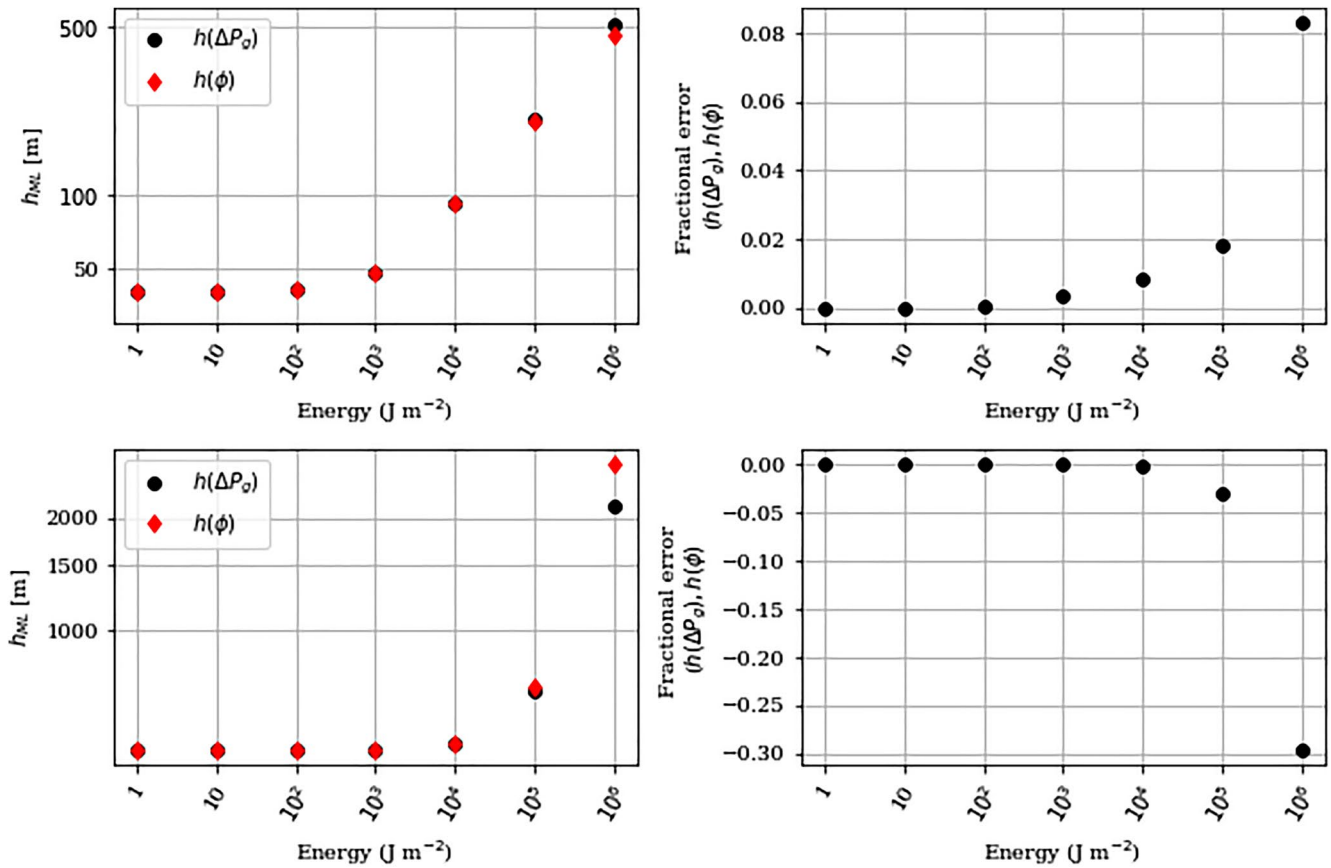


**Figure 6.** Variation of the computed value of $h_{ML}$ with different supplied energies using both $\phi$ (black) and $\Delta P_g$ (red) for (Upper panels) the red-dashed profile from Figure 5 and (Lower panels) the blue-dotted profile. The symbols lie on top of each other for values less than $10^4$ J m$^{-2}$. (Right panels) The fractional error of the $\phi$ method relative to $\Delta P_g$ as a function of supplied energy.

full calculation of $\Delta P_g$ is recommended. We note that this finding is relevant for general use of PE anomaly as a metric, and not just mixed layer analysis.

### 4.2. Case Studies From Two Argo Floats

We now compare the impact of the PE based MLD relative to the threshold and HT09 methods using a time series of $\Theta$, $S$, $p$ measurements from two Argo floats. We chose floats from dynamically distinct regions in the Southern Ocean (ID: 3900660) and Equatorial Pacific (ID: 5904545) to highlight the behavior of the calculation in two very different settings. For all calculations here we use an energy value of 10 J m$^{-2}$ for the PE based methods.

We first focus on the Southern Ocean float 3900660, which yields relatively deep MLDs due to the low surface temperature and weak vertical stratification (Figure 7). This float records several deep mixed layers in the winter, particularly near the beginning of its operation when it reached its southernmost latitude approaching 60°S. The float observed MLDs approaching or exceeding 200 m as observed by the various methods to compute $h_{ML}$ (upper-right). The threshold and HT09 algorithm methods estimate three events with MLDs approaching 400–500 m, while the energy based method only approaches 400 m for the profiles around profile number 200.

We plot the value $h_{ML}$ for each profile diagnosed from the $\Delta P_g$ method against the value diagnosed from the $\phi$, threshold, and HT09 algorithm methods (lower left panel, dots). There is strong agreement between the $\phi$ and $\Delta P_g$ methods, supporting the finding using idealized profiles that it is accurate for MLD calculations to use $\phi$ instead of $\Delta P_g$. However, there are significant differences between $h_{ML}$ from the energy methods versus the threshold and HT09 algorithm methods. These differences are consistent with the range of values of $\phi$ found using the gridded global product (Figures 3 and 4). We summarize the results by a quantile-quantile (Q-Q,

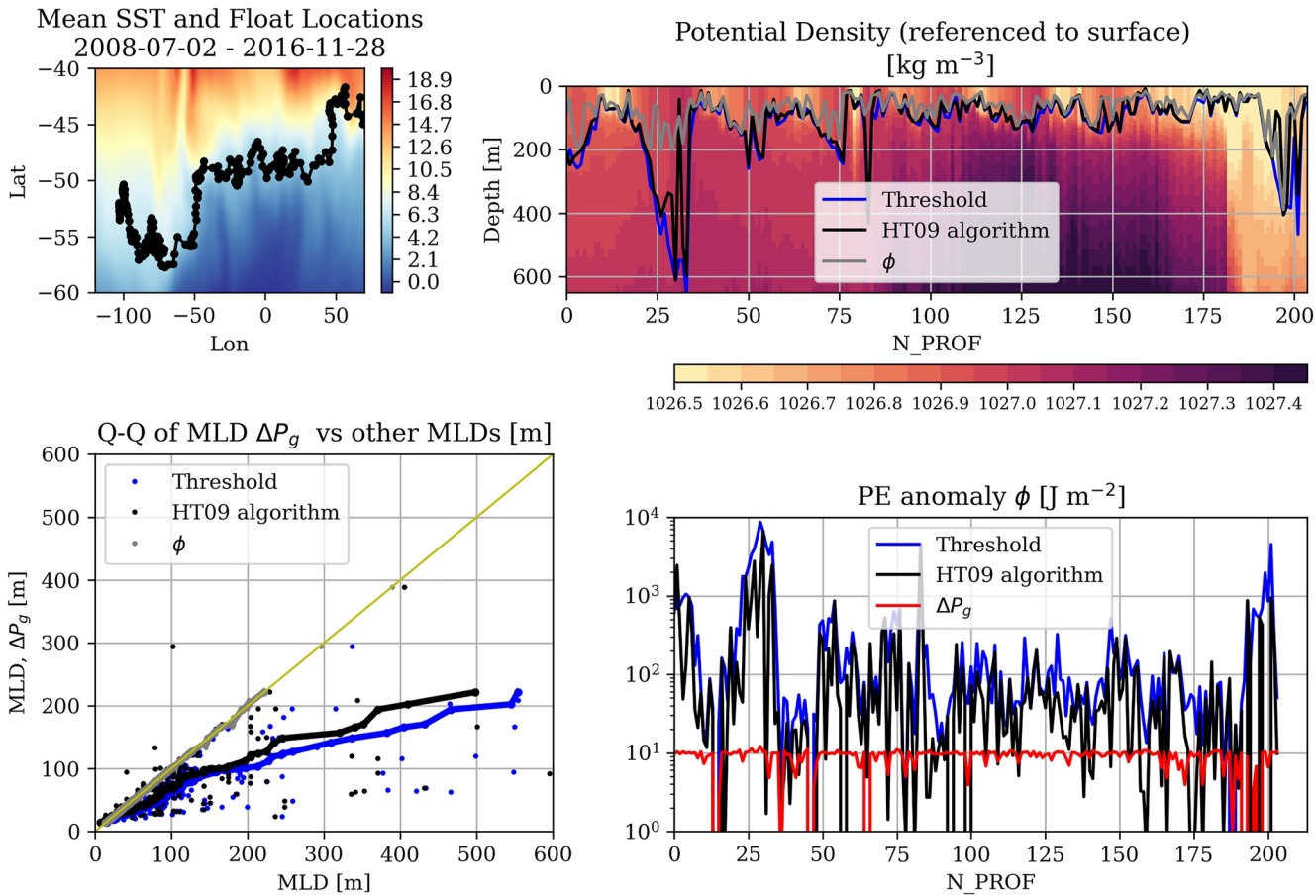


**Figure 7.** (Upper-left) Track of Float 3900660 between 2008 and 2016 with mean SST from https://psl.noaa.gov/data/gridded/data.noaa.oisst.v2.html. Upper right: mixed layer depth (MLD) versus profile number (after QC) from the threshold (blue), HT09 algorithm (black), and $\phi$ (gray) methods, with potential density time-series in the colormap. The $\Delta P_g$ line is omitted because it would be difficult to distinguish from the $\phi$ line. Lower-left: MLD from the $\Delta P_g$ method versus MLD from the other three methods with colors corresponding to the upper-right panel. The raw data is shown in dots while the statistics are shown with Q-Q values in the lines (e.g., plotting values from the PDF from 1% to 99%). Lower-right: PE anomaly of the mixed layer using the threshold, HT09, and $\Delta P_g$ methods to compute the MLD. Note the log-scale for the *y*-axis.

plotting values from the PDF from 1% to 99%) comparison between the methods (bottom left, solid lines). The Q-Q comparison also yields consistently deeper values of $h_{ML}$ from the threshold and HT09 algorithm methods compared to the PE methods across the full range of percentiles. The range of PE anomalies, $\phi$ for the threshold and HT09 methods (bottom right) further emphasize that the mixed layers defined from the standard methods yield significant variability in PE anomaly for the mixed layer, spanning several orders of magnitude. The PE anomaly $\phi$ for the $\Delta P_g$ based method is very close to 10 J m$^{-2}$, further emphasizing the close agreement between the two methods.

We next show the same results for equatorial Argo float 5904545, which spent the majority of its operation between 5°S and the equator, tracking the edge of the Pacific cold tongue (Figure 8). Despite being in a different dynamical regime, the results from this float are similar to those for float 3900660 above. One difference is that the MLDs from 5904545 are much shallower on average. Because the MLDs are shallower, the energy based methods are more consistent with the threshold and HT09 algorithm methods (see particularly the agreement below about 30 m in the Q-Q plot, lower-left solid lines). However, the threshold and HT09 algorithm methods still yield a deeper $h_{ML}$ than the energy methods for the deepest months (particularly for the Q-Q comparison). The range of PE anomalies, $\phi$, for the threshold and HT09 methods (bottom right) again shows significant variability in PE anomaly for the mixed layer.

This analysis from individual Argo floats emphasize similar points found using the gridded datasets. The traditional methods yield mixed layers with significant variability in PE anomaly, suggesting a very different

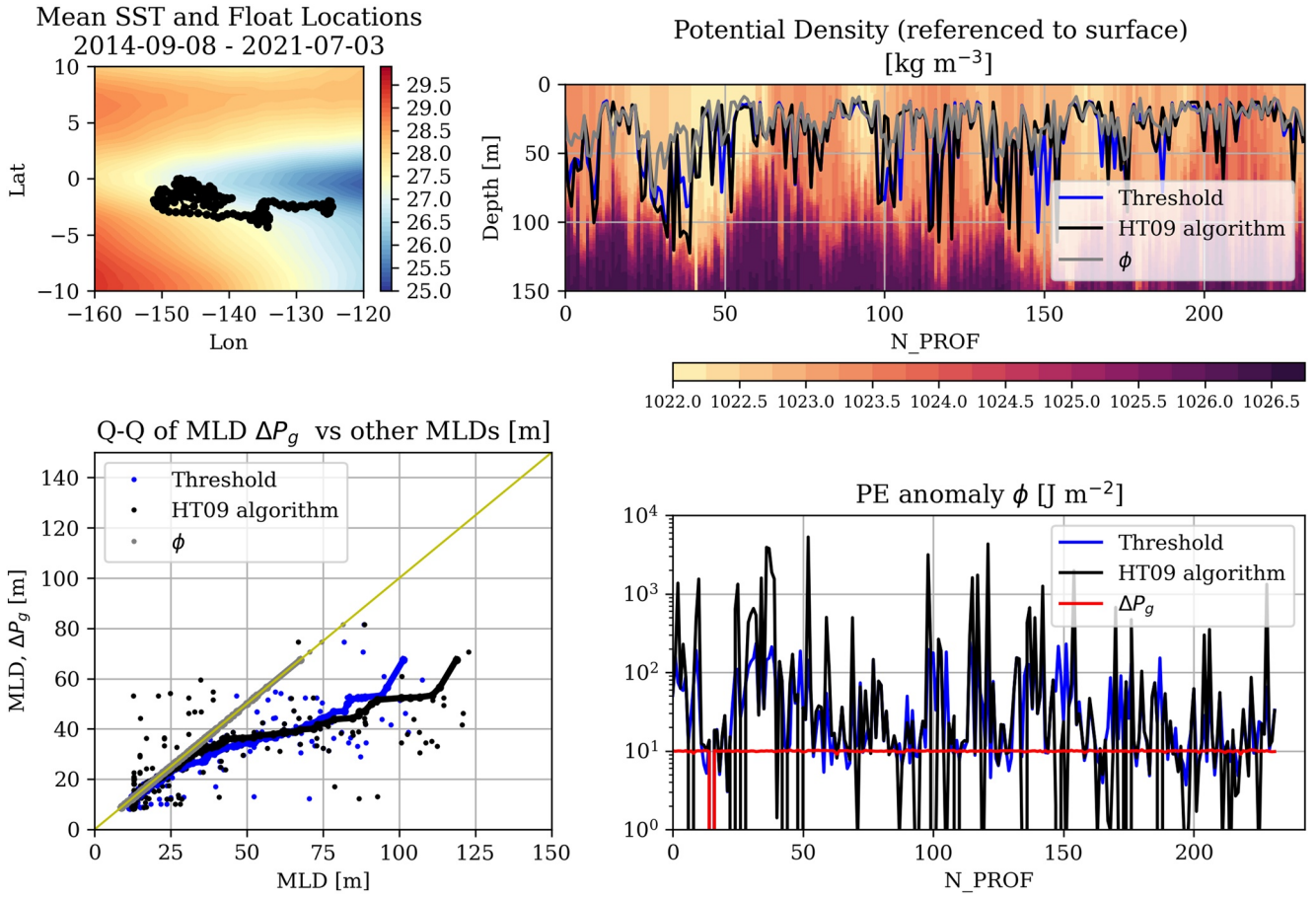


**Figure 8.** (Upper-left) Track of Float 5904545 between 2014 and 2020 with mean SST from https://psl.noaa.gov/data/gridded/data.noaa.oisst.v2.html. (Upper right) mixed layer depth (MLD) versus profile number (after QC) from the threshold (blue), HT09 algorithm (black), and $\phi$ (gray) methods, with potential density time-series in the colormap. The $\Delta P_g$ line is omitted because it would be difficult to distinguish from the $\phi$ line. (Lower-left) MLD from the $\Delta P_g$ method versus MLD from the other three methods with colors corresponding to the upper-right panel. The raw data is shown in dots while the statistics are shown with Q-Q values in the lines (e.g., plotting values from the PDF from 1% to 99%). (Lower-right) potential energy anomaly of the mixed layer using the threshold, HT09, and $\Delta P_g$ methods to compute the MLD. Note the log-scale for the *y*-axis.

stratification occurs within similar mixed layer depths. The PE based methods constrain the PE anomaly, thus yielding a metric with more consistent integrated stratification within the mixed layer.

### 4.3. Sensitivity of the MLD to the Energy Value

We now discuss the sensitivity of the $\phi$-based MLD to the chosen value of $\phi$. Since we already showed that the difference between $\Delta P_g$ and $\phi$ is small for diagnosing surface mixed layers, we only consider $\phi$ in this section.

We first show the resulting 10th percentile (Figure 9) and 90th percentile (Figure 10) of the time series of MLD globally using $\phi$ = 1, 10, 25, and 100 J m$^{-2}$. The $\Theta$, $S$ profiles for this exercise use the Roemmich and Gilson (2009) monthly binned Argo data discussed previously (Section 3.1.3). We compare the global means and the spatial patterns to confirm that a value between 10 and 25 J m$^{-2}$ yields an MLD consistent with the threshold and HT09 algorithm methods for the summer (10th percentile) MLDs (see Figure 3). For the winter (90th percentile) MLDs (see Figure 4), we find an energy value around 100 J m$^{-2}$ or more would be needed to match the global mean MLDs from the threshold and HT09 algorithm methods. We therefore suggest choosing a value of $\phi$ between 10 and 25 J m$^{-2}$ to find MLDs most consistent with the threshold and HT09 methods, but for different applications smaller or larger values may be appropriate. For reference, 10 J m$^{-2}$ of kinetic energy is converted to PE when a 15 m/s wind blows over a section of ocean for about 1 hour (see Appendix B for more context of these energy values).

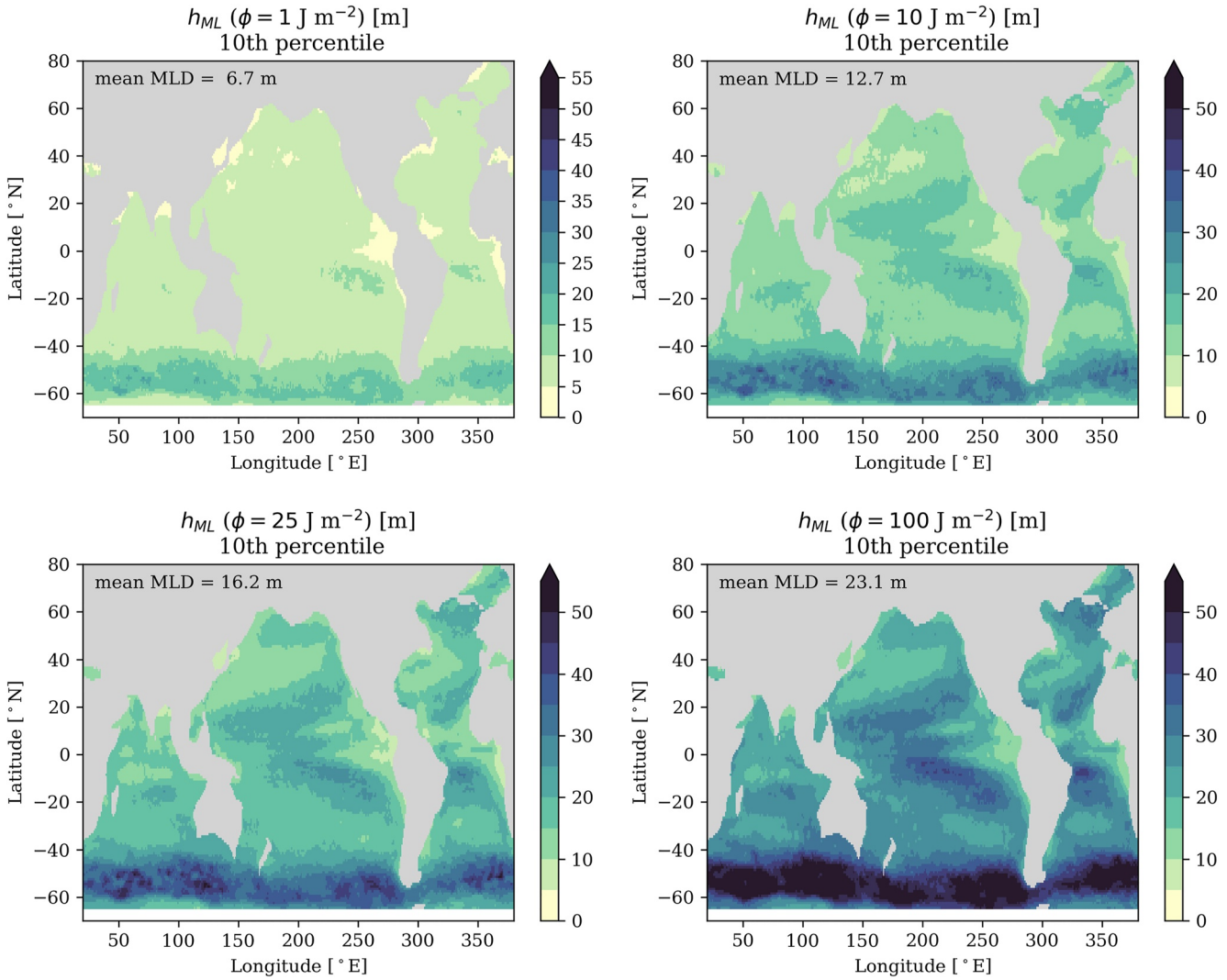


**Figure 9.** Maps of 10th percentile (representing Summer conditions) $h_{ML}$ predicted from values of 1, 10, 25, and 100 J m$^{-2}$ from the $\phi$-based method.

In some regions, if the mixed layer is taken to represent a layer with the potential for turbulent mixing, then greater or smaller energy values may be useful for specific mixed layer analysis. For example, the Southern Ocean typically has high winds and significant buoyancy loss in the winter, meaning TKE levels are usually elevated. Therefore, the estimate of the mixed layer in this region could allow for a stronger degree of inhomogeneity within the MLD, and hence a larger energy value. The specific values of $\phi$ for more specific applications and how these relate to boundary layer depths will be explored further in future studies.

### 4.4. Comparing the Complexity of the Methods

The final comparison we investigate is the computational runtime, which is taken as a proxy for complexity of the different methods. For this experiment we implemented a Python version of the Holte and Talley (2009) MATLAB algorithm to compare with the threshold and energy based calculations. The codes used in this manuscript are all vectorized for performance across *Nd* arrays of profiles in one operation, which improves their efficiency to compute many MLDs in a single pass. However, in this timing exercise we step through the Argo arrays one profile ($1d$) at a time to report an average calculation per profile.

The energy based methods solve for $h_{ML}$ from the bounds of an integral (Equations 16 and 17), so we iterate to find $h_{ML}$ within some threshold. The iteration adds cost to the calculation, so we explore both a bisection iteration

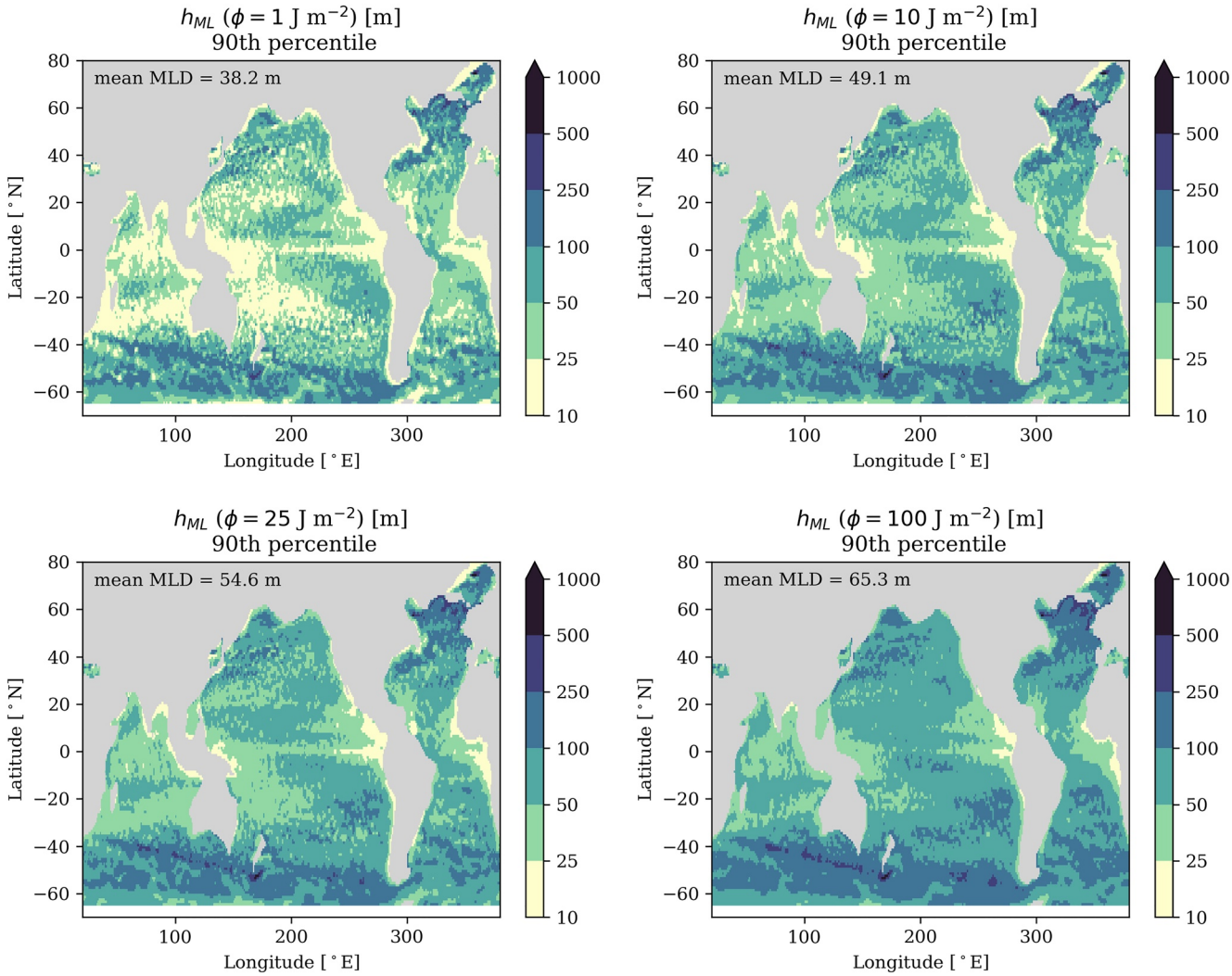


**Figure 10.** Maps of 90th percentile (representing Winter conditions) $h_{ML}$ predicted from values of 1, 10, 25, and 100 J m$^{-2}$ from the $\phi$-based method.

and a slightly more complex Newton's method iteration to evaluate the $\phi$ based MLD calculation. The bisection iteration continuously cuts the column in half to search for a solution and is straightforward to implement for both the $\phi$ and $\Delta P_g$ based methods. The $\phi$ based method is simpler and so we also implement a Newton's method iteration (with some manipulation to the $\Delta P_g$ approach it can also be approached with improved iteration methods). Newton's method almost always converges after one iteration to a fractional precision of energy less than $10^{-5}$ of the prescribed value of $\phi$. The bisection convergence usually takes several iterations, depending on the vertical resolution at which the potential density profile is defined.

We can see from the results (Table 2) that the simplicity of the threshold method yields the smallest runtime per profile, which is consistent with one justification for its standard use. The HT09 algorithm method is by far the slowest in both of these runs. The HT09 algorithm's runtime is primarily spent in a single step, where it estimates the MLD by computing the intersection of linear fits between the surface and interior profiles. The comparison between using $\phi$ and $\Delta P_g$ shows that $\phi$ saves about 2-3x the computation from the full PE calculation in $\Delta P_g$. This increase in calculation time for $\Delta P_g$ is primarily because there is a second field to homogenize and because the non-linear equation of state is called multiple times. The $\Delta P_g$ runtime may be reduced through a local linearization of the equation of state, without significant impact on its accuracy (as is done, e.g., by the ePBL boundary layer parameterization of Reichl and Hallberg (2018)). Switching from the bisection to Newton's iteration also introduces an additional 2-3x speed up. Using the energy based method to estimate

**Table 2**
*Timing per Profile of Argo Calculations for 204 Quality Controlled Profiles From Float 3900660 and 209 Quality Controlled Profiles From Float 5904545*

| Method | Argo 3900660 | Argo 5904545 |
|---|---|---|
| Threshold | 0.0005 s | 0.0010 s |
| HT09 Algorithm | 0.0783 s | 0.9321 s |
| $\phi$, bisection | 0.0029 s | 0.0037 s |
| $\Delta P_g$, bisection | 0.0057 s | 0.0100 s |
| $\phi$, Newton | 0.0013 s | 0.0021 s |

*Note*. The timing experiment was performed 10 times across the full set of profiles and the average is reported. The vertical resolution of the two floats differs from 72 levels in 3900660 to 1055 levels in 5904545, which slows the calculation in the equatorial region despite the shallower MLDs (which are usually proportionally quicker to find).

the MLD is therefore only about a factor of two slower than the threshold method, and is significantly faster to implement than the HT09 algorithm.

## 5. Discussion and Conclusions

We propose here to use the gravitational PE to define the MLD. Since the mixed layer is a region with low stratification due to high mixing, this definition is linked to physical processes in boundary layer turbulence theory. The PE-based method works by estimating the depth to which a given energy could homogenize a layer of seawater. This approach offers conceptual benefits compared to traditional methods since it measures the integrated stratification over a given depth.

We explore two methods to compute the PE difference between a well-mixed layer and its current state. The first method uses the exact temperature and salinity based calculations, and the second uses a simpler "PE anomaly" approach from the potential density. In general, we find the simpler approach to solve for the MLD from the PE anomaly (Equation 17) is sufficient for most surface mixed layer studies.

We also discuss the appropriate range of values of $\phi$, or the amount of energy prescribed, for defining a typical mixed layer. We find that energies in the range of 10–25 J m$^{-2}$ yield MLDs that are generally consistent with previous methods in typical conditions. However, considering multiple $\phi$ values is often useful, as it can provide PE-based information about the stratification over a variety of extents. Larger values of $\phi$ can yield information about how deep larger mixing events may penetrate, which may be useful in certain regions and seasons.

Since the proposed PE-based method is motivated by boundary layer theory, the MLD it yields is more consistent with the BLD from turbulent mixing parameterizations (e.g., Reichl & Hallberg, 2018). Therefore, alternative strategies to choose a value for $\phi$ that is optimized against the BLD from a turbulence perspective will be explored in future studies. Preliminary analysis from climate model output indicates that a value around 15 J m$^{-2}$ yields MLDs roughly consistent with typical BLD values. This preliminary analysis also indicates that the PE-based MLD is significantly better correlated with BLD variability than traditional methods. In this study we do not discriminate between the TKE sources for mixing and the definition of the MLD, but doing so could connect the MLD even more directly to the BLD.

We find that the PE-based MLD is usually consistent with other methods (e.g., the potential density threshold method and HT09 algorithm method) for shallower mid-latitude MLDs such as found in the summer time. However, in winter time the PE-based MLDs are consistently much shallower than the threshold and HT09 MLDs (especially at higher-latitudes). A previous study (Noh & Lee, 2008) finds that the deeper threshold based winter MLDs are less correlated with the depth of the active turbulence BLD. In contrast, our proposed PE-based MLD is better correlated with the BLD in both shallow and deep mixed layers in our preliminary analysis, justifying its use to define the MLD in both regimes. Furthermore, traditional threshold based methods are often difficult to implement in extremely shallow MLD regions such as occur in the Arctic due to large sensitivity to the threshold value and choice for the reference depth. In contrast, the PE-based MLD can be implemented in the same manner globally, with a clear interpretation of the result.

One motivation for the PE-based method is for climate model analysis and evaluation, where computational requirements are a significant concern. We find that the PE-based method is only slightly more complex to implement than the common threshold methods, and it is much simpler than HT09 algorithm method (e.g., based on runtime reported in Table 2). Hence, the PE-based method can be used to identify mixed layer depths from Argo floats and to produce gridded climatologies, which can be used for numerous oceanographic applications. In particular, because the PE-based method defines a MLD that is more consistent with the BLD, we propose its use as a metric to evaluate boundary layer turbulence mixing schemes in numerical models.

## Appendix A: Comments on the Boussinesq Approximation

Many numerical ocean models utilize the Boussinesq approximation to formulate their governing equations. Hence, we here comment on the application of the potential energy (PE) method to a Boussinesq fluid. The flow in a Boussinesq fluid satisfies the incompressible continuity equation, $\partial u_i/\partial x_i = 0$, and scalar diffusion applies to the volume-weighted mean of scalars (including temperature and salinity), rather than the mass-weighted mean. Hence, the Boussinesq fluid does not change its volume during mixing. Instead, the Boussinesq fluid changes its total mass when evaluated from the resulting in situ density evolution. The absence of mass conservation means that a dependence of $\Delta P_g$ on the reference state $z_r$ no longer exactly drops out. This lack of cancellation is demonstrated by noting that

$$\int_{-h}^{\eta_i} \rho_i \, dz = \int_{-h}^{\eta_m} \rho_m \, dz \neq \int_{-h}^{\eta_i} \rho_m \, dz, \tag{A1}$$

for a general equation of state. The first relation in Equation A1 considers the change in the volume in response to going from $\rho$ to $\rho_m$, while the second form that applies to a Boussinesq fluid has a fixed volume. The absence of explicit mass conservation demonstrates that a Boussinesq fluid cannot be treated through the usual definition of PE change from the in situ mean density and its homogenized form. The emergence of $z_r$ as a relevant parameter is an error associated with applying the non-Boussinesq energetics to the Boussinesq fluid, and we do not seek an equivalent solution for this metric in the Boussinesq framework. The optimal solution may also consider the dynamic potential enthalpy, which is a thermodynamic potential needed to close the Boussinesq mechanical energy budget with a pressure dependent equation of state (Young, 2010).

## Appendix B: Understanding the Energy Values

The PE-based mixed layer depth method requires specifying an energy amount to mix the column. Here we provide some physical context for the energy values included in this paper. The energy flux into mixing from the wind is often parameterized from:

$$E_f = m_* u_*^3, \tag{B1}$$

where $u_*$ is the wind friction velocity. The wind friction is often parameterized from a drag coefficient $C_d$ as

$$u_* = \sqrt{C_d \ (\rho_a/\rho_0)}\, U_{10}, \tag{B2}$$

where $U_{10}$ is the mean, neutral ten-meter wind speed and $\rho_a$ is a mean air density. The drag coefficient is usually taken to vary with wind speed and other factors, but since we are only interested in order of magnitude values here we use a constant value of $C_d = 0.0015$. The value of $m_*$ also varies with forcing conditions (Reichl & Hallberg, 2018), but for simplicity here we choose a constant value of $m_* = 0.4$.

We use the wind-driven mixing energy as a guide to offer physical intuition for the energy values presented in this manuscript. In Figure B1 we provide the amount of energy into mixing for wind durations of 1 hr (left), 1 day (middle), and 1 year (right) as a function of the wind speed. From the left panel we see that 10 J m$^{-2}$ of energy is roughly provided to mixing from about one hour of a moderate wind (15 m s$^{-1}$). From the center panel we see that 100 J m$^{-2}$ of energy is roughly provided to mixing from about one day of a moderate wind (12 m s$^{-1}$). From the right panel we see that $10^6$ J m$^{-2}$ of energy would take one year of consistent high wind (35 m s$^{-1}$). This emphasizes that 10–100 J m$^{-2}$ of energy is plausible for mixing throughout much of the ocean during moderate wind events, while $10^6$ J m$^{-2}$ would require extreme duration of high winds. While we focus on wind input to provide physical context, energy can also be provided for mixing from other sources such as surface wave breaking and by PE release during intense convection.

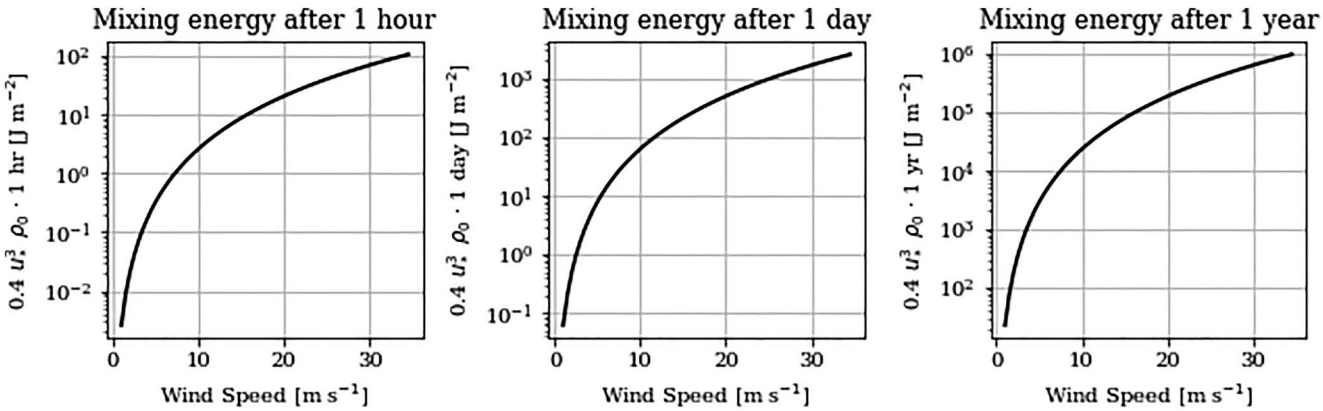


**Figure B1.** Estimates for the time required to provide a given amount of energy to turbulent mixing based on the wind speed and the current speed. The left panel is in units of hours for 10 J m$^{-2}$ of energy, the center panel is in units of days for 100 J m$^{-2}$, and the right panel is in units of days for $10^6$ J m$^{-2}$ of energy. Note the colorbars are logarithmic.

## Data Availability Statement

All Python codes for computing the mixed layer depth using the various methods described in this manuscript are developed at https://github.com/breichl/oceanmixedlayers, the versions used in this work are available on Zenodo at https://doi.org/10.5281/zenodo.6546795. Scripts to generate all Figures including data that is not otherwise available can be found at https://doi.org/10.5281/zenodo.6546929. The Argo data were collected and made freely available by the International Argo Program and the national programs that contribute to it (https://argo.ucsd.edu, https://www.ocean-ops.org). The Argo Program is part of the Global Ocean Observing System. We presented results obtained from the Argo float data and metadata from Global Data Assembly Centre (Argo GDAC)—Snapshot of Argo GDAC of 10 July 2021 (SEANOE) https://doi.org/10.17882/42182#86141. NOAA_OI_SST_V2 data provided by the NOAA/OAR/ESRL PSL, Boulder, Colorado, USA, from their Web site at https://psl.noaa.gov/data/gridded/data.noaa.oisst.v2.html.

**Acknowledgments**
A. Adcroft was supported by Award NA18OAR4320123 from the National Oceanic and Atmospheric Administration, U.S. Department of Commerce. The statements, findings, conclusions, and recommendations are those of the author(s) and do not necessarily reflect the views of the National Oceanic and Atmospheric Administration, or the U.S. Department of Commerce. We thank Graeme MacGilchrist and Marion Alberty for helpful comments during internal reviews on this manuscript. We thank Lars Umlauf, Lars Arneborg, and Hans Burchard for comments and suggestions that improved this manuscript.

## References

Brainerd, K. E., & Gregg, M. C. (1995). Surface mixed and mixing layer depths. *Deep Sea Research Part I: Oceanographic Research Papers*, *42*(9), 1521–1543. https://doi.org/10.1016/0967-0637(95)00068-H

Burchard, H. (2001). On the q$^2$l equation by Mellor and Yamada (1982). *Journal of Physical Oceanography*, *31*(5), 1377–1387. https://doi.org/10.1175/1520-0485(2001)031<1377:OTQLEB>2.0.CO;2

Burchard, H. (2002). Energy-conserving discretisation of turbulent shear and buoyancy production. *Ocean Modelling*, *4*(3–4), 347–361. https://doi.org/10.1016/S1463-5003(02)00009-4

Burchard, H., & Hofmeister, R. (2008). A dynamic equation for the potential energy anomaly for analysing mixing and stratification in estuaries and coastal seas. *Estuarine, Coastal and Shelf Science*, *77*(4), 679–687. https://doi.org/10.1016/j.ecss.2007.10.025

D'Asaro, E. A. (2014). Turbulence in the upper-ocean mixed layer. *Annual Review of Marine Science*, *6*(1), 101–115. (PMID: 23909456). https://doi.org/10.1146/annurev-marine-010213-135138

de Boyer Montégut, C., Madec, G., Fischer, A. S., Lazar, A., & Iudicone, D. (2004). Mixed layer depth over the global ocean: An examination of profile data and a profile-based climatology. *Journal of Geophysical Research*, *109*(C12), C12003. https://doi.org/10.1029/2004JC002378

Feistel, R. (2008). A Gibbs function for seawater thermodynamics for -6 to 80 deg C and salinity up to 120 g/kg. *Deep Sea Research Part I: Oceanographic Research Papers*, *55*(12), 1639–1671. https://doi.org/10.1016/j.dsr.2008.07.004

Franks, P. J. S. (2014). Has Sverdrup's critical depth hypothesis been tested? Mixed layers vs. turbulent layers. *ICES Journal of Marine Science*, *72*(6), 1897–1907. https://doi.org/10.1093/icesjms/fsu175

Gardner, W. D., Chung, S. P., Richardson, M. J., & Walsh, I. D. (1995). The oceanic mixed-layer pump. *Deep Sea Research Part II: Topical Studies in Oceanography*, *42*(2), 757–775. https://doi.org/10.1016/0967-0645(95)00037-Q

Gaspar, P., Grégoris, Y., & Lefevre, J.-M. (1990). A simple eddy kinetic energy model for simulations of the oceanic vertical mixing: Tests at station Papa and Long-Term Upper Ocean Study Site. *Journal of Geophysical Research*, *95*(C9), 16179–16193. https://doi.org/10.1029/JC095iC09p16179

Ginis, I. (2002). Tropical cyclone-ocean interactions. *Advances in Fluid Mechanics Series*, *33*.

Griffies, S. M., Danabasoglu, G., Durack, P. J., Adcroft, A. J., Balaji, V., Böning, C. W., et al. (2016). OMIP contribution to CMIP6: Experimental and diagnostic protocol for the physical component of the Ocean Model Intercomparison Project. *Geoscientific Model Development*, *9*(9), 3231–3296. https://doi.org/10.5194/gmd-9-3231-2016

Groeskamp, S., Griffies, S. M., Iudicone, D., Marsh, R., Nurser, A. G., & Zika, J. D. (2019). The water mass transformation framework for ocean physics and biogeochemistry. *Annual Review of Marine Science*, *11*(1), 271–305. https://doi.org/10.1146/annurev-marine-010318-095421

Holte, J., & Talley, L. (2009). A new algorithm for finding mixed layer depths with applications to Argo data and Subantarctic Mode Water formation. *Journal of Atmospheric and Oceanic Technology*, *26*(9), 1920–1939. https://doi.org/10.1175/2009JTECHO543.1

Hosoda, S., Ohira, T., Sato, K., & Suga, T. (2010). Improved description of global mixed-layer depth using Argo profiling floats. *Journal of Oceanography*, *66*(6), 773–787. https://doi.org/10.1007/s10872-010-0063-3

Kraus, E. B., & Turner, J. S. (1967). A one-dimensional model of the seasonal thermocline II. the general theory and its consequences. *Tellus*, *19*(1), 98–106. https://doi.org/10.1111/j.2153-3490.1967.tb01462.x

Kundu, P., & Cohen, I. (2007). *Fluid mechanics*. Elsevier Science. Retrieved from https://books.google.com/books?id=1a3s9V1ph-0C

Large, W. G., McWilliams, J. C., & Doney, S. C. (1994). Oceanic vertical mixing: A review and a model with a nonlocal boundary layer parameterization. *Reviews of Geophysics*, *32*(4), 363–403. https://doi.org/10.1029/94RG01872

Levitus, S. (1982). *Climatological atlas of the world ocean (Tech. Rep.)*. NOAA/ERL GFDL. (Professional Paper 13).

Lozovatsky, I., Roget, E., Fernando, H., Figueroa, M., & Shapovalov, S. (2006). Sheared turbulence in a weakly stratified upper ocean. *Deep Sea Research Part I: Oceanographic Research Papers*, *53*(2), 387–407. https://doi.org/10.1016/j.dsr.2005.10.002

Lukas, R., & Lindstrom, E. (1991). The mixed layer of the western equatorial Pacific Ocean. *Journal of Geophysical Research*, *96*(S01), 3343–3358. https://doi.org/10.1029/90jc01951

Luyten, J. R., Pedlosky, J., & Stommel, H. (1983). The ventilated thermocline. *Journal of Physical Oceanography*, *13*(2), 292–309. https://doi.org/10.1175/1520-0485(1983)013<0292:TVT>2.0.CO;2

Noh, Y., & Lee, W. (2008). Mixed and mixing layer depths simulated by an OGCM. *Journal of Oceanography*, *64*(2), 217–225. https://doi.org/10.1007/s10872-008-0017-1

Omand, M. M., D'Asaro, E. A., Lee, C. M., Perry, M. J., Briggs, N., Cetinić, I., & Mahadevan, A. (2015). Eddy-driven subduction exports particulate organic carbon from the spring bloom. *Science*, *348*(6231), 222–225. https://doi.org/10.1126/science.1260062

Osborn, T. R. (1980). Estimates of the local rate of diffusion from dissipation measurements. *Journal of Physical Oceanography*, *10*(1), 83–89. https://doi.org/10.1175/1520-0485(1980)010<0083:EOTLRO>2.0.CO;2

Peralta-Ferriz, C., & Woodgate, R. A. (2015). Seasonal and interannual variability of pan-Arctic surface mixed layer properties from 1979 to 2012 from hydrographic data, and the dominance of stratification for multiyear mixed layer depth shoaling. *Progress in Oceanography*, *134*, 19–53. https://doi.org/10.1016/j.pocean.2014.12.005

Price, J. F., Weller, R. A., & Pinkel, R. (1986). Diurnal cycling: Observations and models of the upper ocean response to diurnal heating, cooling, and wind mixing. *Journal of Geophysical Research*, *91*(C7), 8411–8427. https://doi.org/10.1029/JC091iC07p08411

Reichl, B. G., & Hallberg, R. (2018). A simplified energetics based planetary boundary layer (ePBL) approach for ocean climate simulations. *Ocean Modelling*, *132*, 112–129. https://doi.org/10.1016/j.ocemod.2018.10.004

Reichl, B. G., & Li, Q. (2019). A parameterization with a constrained potential energy conversion rate of vertical mixing due to Langmuir turbulence. *Journal of Physical Oceanography*, *49*(11), 2935–2959. https://doi.org/10.1175/JPO-D-18-0258.1

Rodi, W. (1987). Examples of calculation methods for flow and mixing in stratified fluids. *Journal of Geophysical Research*, *92*(C5), 5305–5328. https://doi.org/10.1029/JC092iC05p05305

Roemmich, D., & Gilson, J. (2009). The 2004-2008 mean and annual cycle of temperature, salinity, and steric height in the global ocean from the Argo Program. *Progress in Oceanography*, *82*(2), 81–100. https://doi.org/10.1016/j.pocean.2009.03.004

Simpson, J. H. (1981). The shelf-sea fronts: Implications of their existence and behavior. *Philosophical Transactions of the Royal Society of London - A*, *302*, 531–546. https://doi.org/10.1098/rsta.1981.0181

Sutherland, G., Reverdin, G., Marié, L., & Ward, B. (2014). Mixed and mixing layer depths in the ocean surface boundary layer under conditions of diurnal stratification. *Geophysical Research Letters*, *41*(23), 8469–8476. https://doi.org/10.1002/2014GL061939

Tennekes, H., & Lumley, J. (1972). *A first course in turbulence*.

Thomson, R., & Fine, I. (2003). Estimating mixed layer depth from oceanic profile data. *Journal of Atmospheric and Oceanic Technology*, *20*(2), 319–329. https://doi.org/10.1175/1520-0426(2003)020<0319:EMLDFO>2.0.CO;2

Williams, R. G. (1991). The role of the mixed layer in setting the potential vorticity of the main thermocline. *Journal of Physical Oceanography*, *21*(12), 1803–1814. https://doi.org/10.1175/1520-0485(1991)021<1803:TROTML>2.0.CO;2

Wong, A. P. S., Wijffels, S. E., Riser, S. C., Pouliquen, S., Hosoda, S., Roemmich, D., et al. (2020). Argo data 1999-2019: Two million temperature-salinity profiles and subsurface velocity observations from a global array of profiling floats. *Frontiers in Marine Science*, *7*, 700. https://doi.org/10.3389/fmars.2020.00700

Yamaguchi, R., Suga, T., Richards, K. J., & Biu, Q. (2019). Diagnosing the development of seasonal stratification using the potential energy anomaly in the north Pacific. *Climate Dynamics*, *53*(7–8), 4667–4681. https://doi.org/10.1007/s00382-019-04816-y

Young, W. R. (2010). Dynamic enthalpy, conservative temperature, and the seawater Boussinesq approximation. *Journal of Physical Oceanography*, *40*(2), 394–400. https://doi.org/10.1175/2009JPO4294.1